NTNU – Trondheim
Norwegian University of
Science and Technology

Drillpipe Rotation Effects on Pressure Losses

Thorbjørn Lejon Skjold

Earth Sciences and Petroleum Engineering
Submission date: June 2012
Supervisor: Pål Skalle, IPT

Norwegian University of Science and Technology
Department of Petroleum Engineering and Applied Geophysics

Abstract

Keeping control of the downhole pressure is important in any drilling situation, and especially when a narrow pressure window is experienced. The equivalent circulation density is influenced by rotation of the drillpipe, but there is no existing mathematical description for this behavior.

In present project, existing knowledge of how drillpipe rotation affects pressure losses was presented, and used as a foundation in the development of empirical equations through regression analysis. Several data sets were gathered from various field studies, and a set of working equations was developed. The equations were presented in two different forms. One equation expressed pressure losses with rotation and without rotation, $\Delta P_{\omega \neq 0}/\Delta P_{\omega=0}$ vs. revolutions per minute. The three other equations describes $\Delta P_{\omega \neq 0}/\Delta P_{\omega=0}$ vs. Reynolds number, for selected rotation speeds.

The four equations were tested for their accuracy by comparing with simulations performed in the software Drillbench®, by comparing with an existing mathematical model, and by comparing with virgin field data. All equations gave predictions close to the existing semi-empirical model. The equation described as a function of RPM predicted a smaller pressure loss ratio than the field study for a rotation speed of 60 RPM, but came within the results from this study for a rotation speed of 120 RPM. The equations expressed as a function of Reynolds number gave results closer to the semi-empirical model than the RPM-equation. All equations predicted a larger pressure loss than the simulations performed in Drillbench®, in some cases even twice as large.

To further improve the equations, larger data sets have to be acquired. The quality of the equations will improve if they cover more situations, and if they are based on a wider spread in the data sets.

Sammendrag

Å holde kontroll på nedi hulls trykk er viktig i alle boresammenhenger, og spesielt når et trangt trykkvindu oppleves. ECD blir påvirket av rotasjon av borestrengen, men det eksisterer ingen matematisk formel som beskriver dette bidraget.

I dette prosjektet ble den eksisterende kunnskap om hvordan rotasjon av borestrengen påvirker trykktap i ringrom presentert og brukt som et grunnlag under utviklingen av empiriske formler gjennom regresjonsanalyse. Datasett ble samlet inn fra flere feltstudier, og et sett av funksjonelle ligninger ble utviklet. Ligningene ble presentert på to ulike former. En ligning uttrykker trykktap med rotasjon og uten rotasjon, $\Delta P_{\omega\neq0}/\Delta P_{\omega=0}$ mot rotasjoner per minutt. De tre andre ligningene beskriver $\Delta P_{\omega\neq0}/\Delta P_{\omega=0}$ mot Reynolds tall, for utvalgte rotasjonshastigheter.

De fire ligningene ble testet for deres nøyaktighet ved å sammenligne med simuleringer i programvaren Drillbench®, ved å sammenligne med en eksisterende matematisk modell, og ved å sammenligne med ubrukt feltdata. Alle ligningene gav resultater nær den eksiterende delvis empiriske modellen. Ligningen som ble beskrevet som en funksjon av rotasjonshastighet anslo lavere rater for trykktap enn feltstudiet for en rotasjonshastighet på 60 rotasjoner per minutt, men kom innenfor intervallet i studiet ved en rotasjonshastighet på 120 rotasjoner i minuttet. Ligningene uttrykt som en funksjon av Reynolds tall gav resultater nærmere den delvis empiriske modellen enn ligningen for rotasjonshastighet. Alle ligningene gav et høyere trykktap enn resultatene fra Drillbench®-simuleringene, i noen tilfeller dobbelt så stort.

For å videreutvikle ligningene er det et behov for større datasett. Kvaliteten på ligningene vil bli bedre dersom de dekker flere situasjoner, og dersom de er utviklet fra datasett med en større spredning.

Table of Contents

List of Figures

List of Tables

Chapter 1: Introduction

Handling of the downhole pressure and its variation is important for various reasons. Both the cleaning aspect and the pressure limitations are of great importance. The added contribution of drillstring rotation on the equivalent circulation density (ECD) can in some situations be of such a magnitude that impossible drilling conditions are experienced. In situations with narrow pressure window, accurate prediction of ECD is crucial, though there is no existing common equation representing the rotational contribution. Up to now, the problem has been solved with a variety of equations developed from specific field experiments, or semi-theoretical equations, but with strong limitations on their usability.

In this thesis, empirical equations of how drillstring rotation is affecting ECD in general will be derived through regression analysis of collected drilling data. The accuracy of these equations will be tested through example calculations by use of a new set of drilling data. In addition, the empirical equations will be compared to an existing semi-empirical equation expressing drillpipe rotation effects and simulations of ECD from the software Drillbench®. This software is chosen on basis of its availability and reputation in the industry. Allthough the software do not reveal its model of rotational effects, it can be helpful in testing the accuracy of the empirical equations developed through present project. The goal of this project is to develop empirical equations for the rotational contribution of ECD and make them applicable to all possible scenarios, with as few simplifications as possible, and without compromising with the limitations of the equation.

To reach this goal, a stepwise approach is needed. The first step will be to acquire enough knowledge on the problematical areas within drillstring rotation, discuss and evaluate the problems, and find possible solutions on how to express them mathematically. Here we will present why field data show increased pressure loss in the laminar area while theoretical evaluation leads to reduced pressure loss. Step two will be to gather a largest possible data bank of pressure vs. rotation during pumping. Step three will consist of data arranging and regression analysis to obtain a set of working equations. The last step will be to test the accuracy and usability of the models, by comparing the equations to real drilling data, the semi-empirical equation, and to the Drillbench® simulations.

Chapter 2: Previous Published Work on Rotational Effects on ECD

This chapter will provide a theoretical foundation for the understanding of drillstring rotational effects on ECD. It is roughly divided into two parts; the first part will provide information of the most important topics that might interfere with drillstring rotational effects and ECD, along with a presentation of pipe rotation in laminar and turbulent fluid flows. The second part will be a presentation of previous published work on drillstring rotation.

2.1: ECD Control: Influence of Annulus Pressure Drops in General

Equivalent circulation density can be understood as the total actual bottomhole pressure exerted on the formation (Skalle 2010), and is the sum of equivalent static density (ESD) and the pressure increments experienced from pressure drops along the annulus, and the extra weight of drill cuttings contained in the annulus. Controlling the ECD is especially important when drilling long, horizontal well sections, deepwater drilling, drilling through depleted reservoirs, and for other wellbores where a narrow pressure window is experienced. From **Fig. 1** and **Fig. 2** it can be seen why controlling ECD is important. Fig. 1 show the ESD gradient for a well drilled in a depleted reservoir, along with the ESD gradient plus the rotational contribution of the ECD, plotted with the pore pressure gradient and fracture pressure gradient versus depth. Fig. 2 shows the plot of the ECD gradient with rotational effects. As can be seen from this figure, the additional pressure increment in ECD causes the bottomhole pressure to exceed the upper pressure limit, leading to impossible drilling conditions.

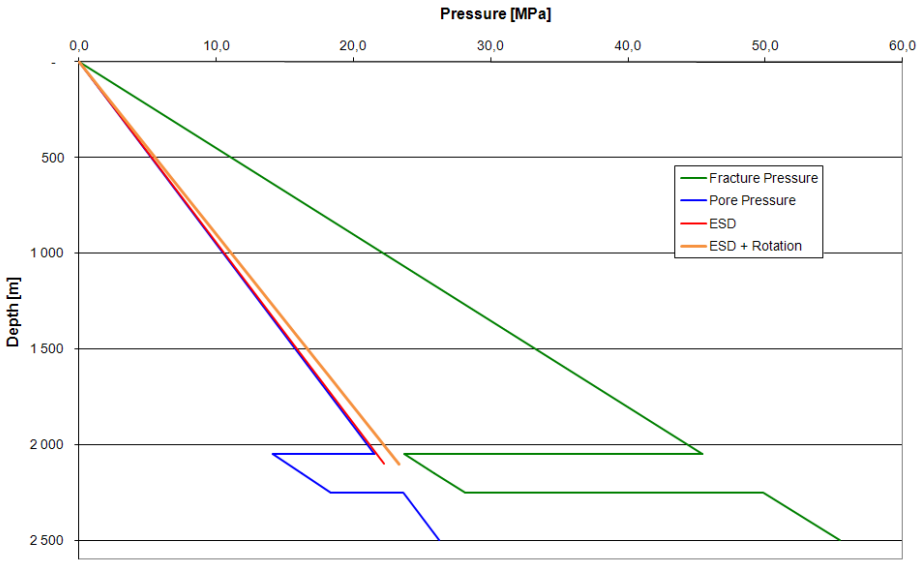

Fig. 1—ESD and rotational effects plotted into pressure window (Skjold 2011).

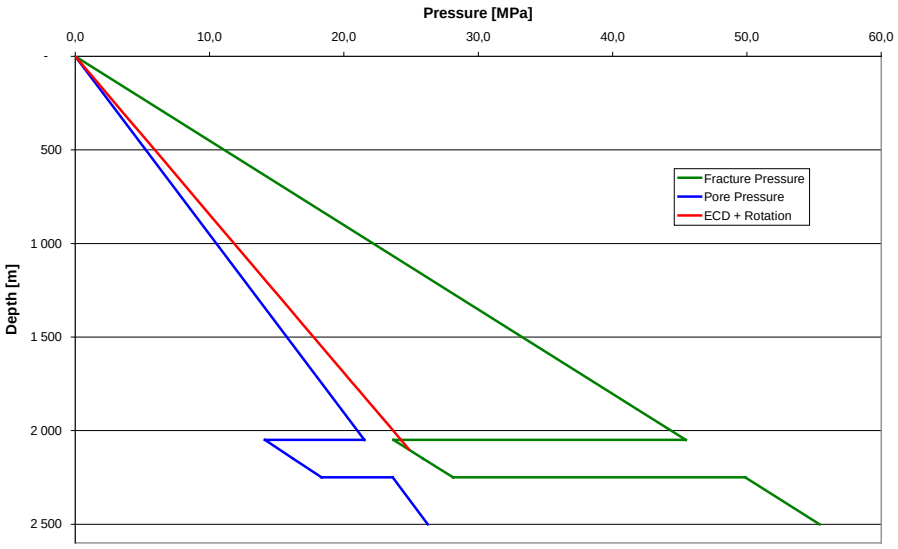

Fig. 2—ECD and rotational effects plotted into pressure window (Skjold 2011).

A general equation to express ECD, with the different pressure drops included, is presented below:

$$ECD = \rho_{mud} + \frac{\Delta p_{friction,annular} + \Delta p_{cuttings} + \Delta p_{surge\&swab} + \Delta p_{rotation} + \Delta p_{acceleration}}{gz} \quad (2.1)$$

As can be seen from the equation, the various pressure increments arise from various sources. Normally the effects of increasing temperature with increasing depth, and increasing hydrostatic pressure with increasing depth, are ignored when calculating ECD (Skalle 2010).

2.1.1: Annular Friction

Pressure loss resulting from annular friction is caused by the fluid's motion against an enclosed surface, such as a pipe (OilGasGlossary 2012). When a fluid is flowing through a pipe, the friction within the fluid and against the pipe wall creates pressure losses. Annular friction is most accurately estimated by selecting the best fitting rheological model, whether this is the Newtonian model, the Bingham model, the Herschel-Buckley model or the Power law model.

2.1.2: Cuttings Effect

In a horizontal well there is a certain amount of cuttings in suspension, and these cuttings contribute with a pressure loss increment. Some of the cuttings settle, some are inside the mud flow, and some are lifted by lifting forces in the mud flow. These cutting amounts affect the

mud weight (MW), and thereby the bottomhole pressure. It is not easy to predict without assuming some of the values, though a set of equations to estimate the pressure loss do exist:

$$\Delta p_{cuttings} = \rho_{cuttings,average} \cdot g \cdot TVD \tag{2.2}$$

In this equation, $\rho_{cuttings,average}$ is expressed by:

$$\rho_{cuttings,average} = \rho_{mud}(1 - c_{cuttings,average}) + \rho_{cuttings} \cdot c_{cuttings,average} \tag{2.3}$$

Rotation of the drillstring will influence this pressure loss by changing how large the cutting beds will be (Skalle 2010).

2.1.3: Surge and Swab

Surge and swab is the term used when talking about pressure changes from tripping operations. When tripping out, the bottomhole pressure will decrease because of friction between the moving pipe and the stationary drilling fluid. This pressure is referred to as swab pressure. A bottomhole pressure increase will be seen when tripping into the hole, referred to as swab pressure (New Mexico Tech 2012). The downward mud movement experienced when tripping out of hole is shown in **Fig. 3**. The green line indicates the mud position before the operation is started, while the red lines indicate how the mud is displacing the void left by the upward movement of the pipe.

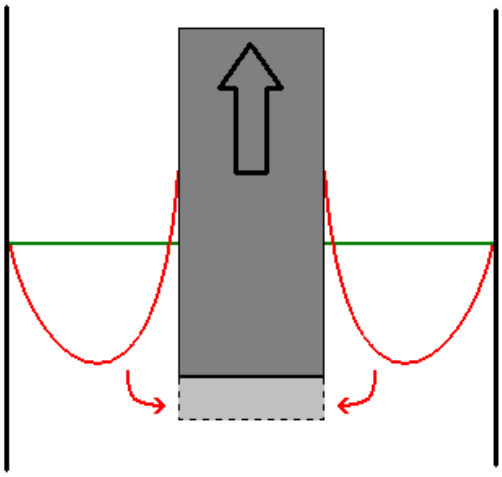

Fig. 3—Fluid movement when tripping out of hole (free after Skalle, 2010).

2.1.4: Gelling

Gelling is the term used for the gelled structure most drilling fluids form while being at rest for a certain amount of time. Before being able to circulate, the gel structure has to be broken, and an extra pressure has to be applied to break the gel on the pipe surface (Skalle 2010). To get the extra pressure needed, either the pump is used, or simply the pipe is rotated. The gel breaking pressure is thought to be small, and hidden in the acceleration pressure.

2.1.5: Acceleration

The acceleration pressure is also caused by pipe movement. It is experienced during some tripping operations, and when a gas kick reaches the surface (Skalle 2010). Acceleration of the pipe causes an acceleration pressure in the drill fluid. This phenomenon is calculated with the following equation:

$$\Delta p_{acceleration} = m \cdot a = \rho \cdot L \cdot a_{pipe} \cdot \frac{A_{pipe,effective}}{A_{ann,effective}} \tag{2.4}$$

2.2: Rotation of Drillstring

Rotation of the drillstring could significantly alter the bottomhole pressure, but a series of studies on pipe rotation show contradictory results of whether this alteration is positive or negative, as will be explained in detail later. As presented by Skalle (2010), pipe rotation in a laminar flow will lead to an additional shear velocity component. Normally drill fluids are shear thinning, and rotation would give an increase in total shear stress, with a decrease of the viscosity, leading to a reduction of the pressure drop and the corresponding bottomhole pressure. When rotating the drillpipe, the effective strain rate is increased, the effective viscosity decreased, with a reduction of the axial pressure drop as a result. In laminar developed flows of Newtonian fluids (see **Fig. 4**), viscosity is independent of shear rate, and the described effects could not take place. At the slowest rotation rates, when both the Reynolds number and the Taylor number are beneath their critical values, the laminar fluid flow could be depicted as a helical type flow.

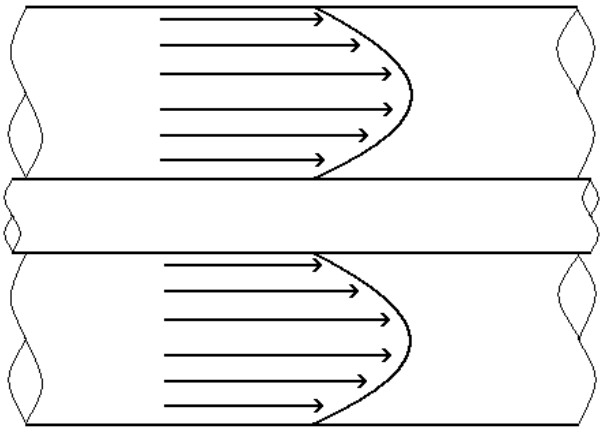

Fig. 4—Laminar fluid flow in the annulus.

For most drilling operations, an increased pressure drop will be experienced. This is thought to be caused by the development of instabilities (Skalle 2010). According to Marken et al. (1992), rotation of the drillstring would create centripetal forces 'throwing' away fluid close to the pipe, leaving a 'void'. These 'voids' are filled with fluid from the outer part of the annulus. As a result, secondary flow called Taylor vortices are created, as shown in **Fig. 5.** As described by Skalle (2010), rotation and the forming of these vortices would lead to an axial-radial mixing, and this would have the same effect on momentum transport as turbulent mixing.

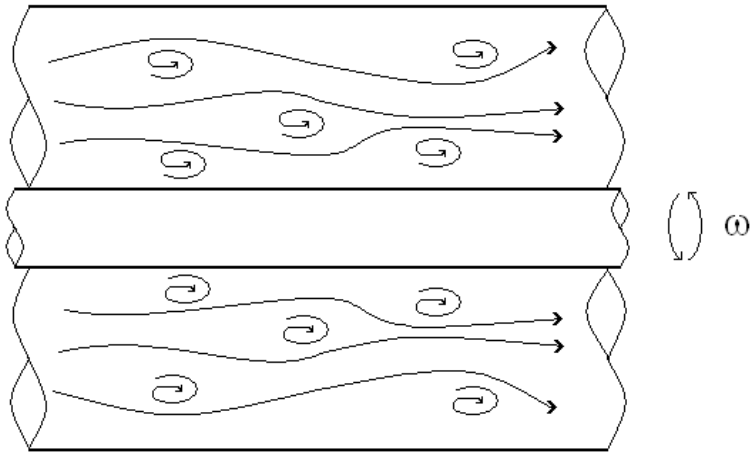

Fig. 5—Formation of Taylor vortices when pipe is rotated resulting in "turbulent-like" mixing.

Because turbulent flow is shear thickening, this effect will lead to an increased pressure drop, as field studies in the next subchapters will present. In addition to the formation of Taylor vortices, Marken et al. (1992) presented some additional suggestions as to what causes the increased pressure drops. During drilling operations with fluid circulation, effects like drillstring vibration and motion of the pipe will alter the flow regimes. Lateral and rotational

motion, along with axial vibration and motion, tend to disrupt fluid flow patterns, giving another contribution to the 'turbulent-like' flow.

2.3: Knowledge from Previous Studies on Rotational Effects

The following sections will reveal existing work regarding rotational effects on ECD. This is done to give a larger foundation to understand why this project is carried out, and will also serve as a reference to the relevance of the project. For this topic, the chapter is divided into two parts, experimental results, and field testing versus theoretical approach. The reason for this classification is to highlight the differences within the results obtained from the various procedures. To clarify how the published studies are classified, an explanation of the terms will now be given. Field testing contains studies based on field measurements, where an actual well have been used to provide the most realistic conditions, but with limitations on the accuracy of measurements and the ability to focus on one single part of the process because of the influence from other phenomenon. An example of field testing is the work of Charlez et al. (1998). The theoretical approach contains, as the name imply, studies from a theoretical point of view. Here the studies are more based on theory, with a biased opinion of the expected results, both from field measurements and from laboratory experiments. An example study of this is Ahmed & Miska (2008). For the experimental approach, laboratory measurements and testing of specific parameters is the criteria. An example of such a study is Hansen & Sterri (1995).

2.3.1: Field Testing vs. Theoretical Approach

A lot of field testing has been carried out to understand how the ECD react to pipe rotation. Pressure-While-Drilling (PWD) was used to obtain data in several extended reach wells (ERD) in the North Sea (Charlez et al. 1998), and this data was used to investigate drillpipe rotation effects on ECD. From a series of drillstring rotation tests, it was found that for a constant flow rate, rotation of the drillpipe would increase close to linearly with the rotation speed. This was found in a 12¼-in. hole with a flow rate of 0.045 m^3/s, and in an 8½-in. hole with constant flow rate of 0.028 m^3/s. In the same test, it could be seen that the increase would be larger in the latter case. Testing was also performed for different flow rates with several rotation speeds. This test shows that flow rate does not change the trend from the first test; an increased ECD will be seen with increased drillstring rotation speed.

These results were supported by Bertin et al. (1998). Through this work it was also found that pipe rotation would have a positive effect on ECD, and that it was almost linear with the pipe revolutions per minute (RPM). The results suggested an ECD increase resulting from pipe rotation of around 10 kg/m^3 for every 60 RPM increase.

A study by Andreassen & Ward (1997) of PWD measurements from Statfjord and Gullfaks also concluded that rotation of the drillstring would lead to an ECD increase, and especially for high rotation speed (above 50 RPM). It was found that depending on the drilling fluid used, rotation could increase the ECD with between 50% and 100% compared to that with no rotation. Rotation speeds less than 50 RPM was found not to give any important contribution to ECD, and this was thought to be owing to the uneven mud weights, and that cutting loads affected the measured data.

Bode et al. (1989) presented a study of slim-hole drilling. Through tests performed in the well, an increased pressure loss could be seen when the drillstring was rotated. The bottomhole ECD showed 12.1 lbm/gal with no rotation, while a rotation speed of 600 RPM increased the ECD value to 16.1 lbm/gal. Another study of slim-hole drilling (Delwiche et al. 1992) also gave an increased pressure loss. In this study, the pressure loss inside annulus because of drillstring rotation was found to be larger for a slim hole compared to a conventional hole, but in both situations an increase was seen.

Other studies show similar results, a narrow borehole will give a larger increase in pressure losses when drillpipe is rotated. McCann et al. (1993) and Haige et al. (2000) conducted experiments on this topic. These results will be thoroughly presented in the next section, but both of the studies gave affirmative results. Diaz et al. (2004) carried out a theoretical study, and compared the expected results with field data. It was found that increasing drillstring rotation speed would lead to increased pressure losses in the annulus. When the annular clearance decreases, an effect like eccentricity will play a larger role for rotational-induced pressure losses than what is the case for a regular wellbore.

A combined theoretical and experimental study was performed by Ahmed & Miska (2008). It was found that for a highly eccentric pipe, rotation indicated presence of shear thinning and

inertial effects, which results in increased pressure losses when the pipe is rotated. The inertial effects could be generated both from eccentricity and from geometric irregularities, or a combination of these. The presence of inertial effects could affect the velocity field when the pipe is rotating.

Ahmed et al. (2010) combined field measurements with the theory of pipe rotation to find a model that could predict the pressure losses as a function of drillpipe rotation. They developed a semi-empirical model, and with dimensionless input parameters for all the theoretical expressions. A full presentation of this study will be given in chapter 3, and this model will later be used to validate the accuracy of the empirical equations developed in this project.

2.3.2: Experimental Results

Hansen & Sterri (1995) concluded that rotation would decrease the frictional pressure loss for a helical flow when Reynolds number is kept smaller than the Taylor number, and the Taylor number is less than the critical Taylor number. However, if the Reynolds number is less than the critical Reynolds number and the Taylor number is above the critical Taylor number, or if both the Reynolds number is greater than the critical Reynolds number and the Taylor number is greater than the critical Taylor number, there will be an increase in the frictional pressure loss.

In a study conducted by McCann et al. (1993), a 1.25 inch steel shaft within a clear acrylic tube of diameter 1.375 to 1.75 inch internal diameter were used for sensitive pressure measurements of fluid flow in a concentric annuli, and a similar test with a clear acrylic tube of 1.50 inches internal diameter were used to make similar measurements for a fully eccentric annuli. During the testing, a maximum rotation speed of 900 RPM and a maximum fluid flow rate of 0.001 m^3/s were used. In this experiment it was found that for a laminar flow, increased pipe rotation would lead to a decreased pressure loss, while for a turbulent flow increased pipe rotation would give a increased pressure loss. The results obtained in this study were compared with typical models used by the industry to predict pressure losses from pipe rotation, and they found that none of them gave satisfying results. It was also seen that increasing mud rheology would give an increased pressure loss, while increasing eccentricity would lead to decreased pressure loss, regardless of the flow regime.

Similar results were found in a study performed by Hansen et al. (1999). Here a steel tube with outer diameter of 4.45 cm was placed inside a transparent Plexiglas tube with inner diameter of 5.08 cm. The steel tube could be placed according to the desired eccentricity of the annulus. The maximum flow rate used in the experiment was 0.008 m^3/s, and a maximum pipe rotation of 600 RPM. The experiment was conducted to study the influence of pipe rotation in narrow annuli for various flow regimes, by use of several fluids, and test the accuracy of existing models for predicting pressure losses. The fluids used were water, different solutions of CMC (Carboxyl Methyl Cellulose) in water, and different solutions of Xanthan in water. Water was found to be a Newtonian fluid, water mixed with CMC was characterized by a two parameter Power law model, water and Xhantan in a mixture would represent a Bingham fluid, or it was described by a three-point Herschel-Bulkley model if the lowest shear rates were neglected.

In the experiments it was found that eccentricity would decrease pressure losses relative to concentric pipe position regardless of the fluid used. Furthermore, for shear thinning fluids such as CMC solutions, it was found that the frictional pressure losses would be reduced when rotating the pipe at low flow rates, while increased pressure losses were seen at higher flow rates.

Another experimental study was conducted by Haige et al. (2000). The testing were performed by use of a transparent outer pipe with an internal pipe diameter of 5 in., and two different diameters on the inner pipe, 3 in. and 3.5 in.. The length of the test apparatus was 6 meters. From the test results it was seen that a slow pipe rotation speed would lead to a small decrease in annular pressure losses. When rotating at speeds above 70 RPM, a rapid increase in annular pressure losses was experienced. It was found that increasing eccentricity would quickly decrease the annular pressure losses. By comparing the results from testing done with the two different inner pipe diameters, it was found that a decreased annular gap would make the pressures much more sensitive to pipe rotation speed.

Chapter 3: The PLR-Equation

The need for a mathematical model of pipe rotation effects on ECD has been presented earlier in this project. An effort to make such a model was done by Ahmed et al. (2010). In this study, a semi-theoretical model was developed based on field studies. The equation obtained was presented in dimensionless parameters, with the introduction of a key parameter, the pressure loss ratio (PLR).

$$PLR = \frac{(dP/dL)_{\omega}}{(dP/dL)_{\omega=0}} \tag{3.1}$$

As can be seen from this equation, the pressure loss ratio is the *pressure loss with pipe rotation* divided by *pressure loss without rotation*. Through dimensionless analysis, the solution to this equation was described as:

$$PLR = 0.36 \times (13.5 + \frac{\tau_y}{\rho U^2})^{0.428} \times \varepsilon_{ave}{}^{0.158} \times n^{0.054} \times Ta^{0.0319} \times \mathrm{Re}_{eff}^{0.042} \times k(\frac{1}{k} - 1)^{-0.0152} \tag{3.2}$$

In this equation, ρ represents the fluid density, τ_y is the Herschel-Bulkley yield stress, and n is the fluid behavior index from this rheology model. Furthermore, U is the mean annular velocity, and k is the diameter ratio between the drillpipe and the borehole wall, D_p/D_h. The other parameters are described with equations. Ta is the Taylor number, described by:

$$Ta = \frac{D_p (D_h - D_p)^3}{16} \left(\frac{\rho \omega}{\mu_{app}} \right)^2 \tag{3.3}$$

In this equation, D_p is the pipe diameter, D_h is the hole diameter, ρ is the fluid density, ω is the angular speed, and μ_{app} the apparent viscosity.

The parameter ε_{ave} is the average dimensionless eccentricity, described by:

$$\varepsilon_{ave} = \sum_{i=1}^{n} \frac{2E_i}{(D_h - D_p)} \frac{L_i}{MD} \tag{3.4}$$

Again, D_h and D_p represents the hole diameter and the pipe diameter respectively. MD is the measured depth, L_i is the length of a wellbore section, and E_i is the effective eccentricity described by:

$$E = \frac{D_h - D_{TJ}}{D_h - D_p} \tag{3.5}$$

D_{TJ} is here the tool joint diameter, and the other parameters are as previously described. E is to be calculated for every wellbore section L_i.

The final parameter to be discribed, is Re_{eff}. This parameter is found with Eq. 3.6:

$$\mathrm{Re}_{eff} = \frac{8\rho U^2}{\tau_{w,lam}} \tag{3.6}$$

This is how the effective Reynolds number is described. U is the mean annular velocity, and ρ is the fluid density. The final parameter to be described is $\tau_{w,lam}$, which is the average wall shear stress for a concentric annulus.

The model presented above was derived by analyzing data from field studies, but some of the studies were omitted because of lacking key parameters required for testing purposes, or data points were withdrawn because of bad correlation. This was done where it was thought that inaccuracies from measurements were causing poor correlation to the other data sets. During model validation, predicted values were compared to measured values from several field studies, and even though the field studies were taken under various drilling conditions, the predictions were fairly accurate, with an error of approximately ±15%.

In the development of the empirical equations later in this project, this theoretical model will be used for comparison purposes, along with the results obtained from the Drillbench® simulations in the next chapter.

Chapter 4: The Drillbench® Software: for Comparison Purposes

This chapter will serve as a presentation of the simulation software used in this project. It consists of two parts, a general description of the software and its possibilities, and a presentation of simulations done based on a field study.

4.1: Presentation of Software

As previously mentioned, the equations developed in this project will be compared to simulations performed in software called Drillbench®. This is a commercial software package owned by the SPT Group. The software suite is used for designing and evaluation of drilling operations. It consists of three modules, Dynamic Hydraulics, Dynamic Well Control and Underbalanced Operations. Each of these modules consists of one or more applications. The Underbalanced Operations-module have two applications, Dynaflodrill and Steadyflodrill, Dynamic Well Control have one application, called Kick, while Dynamic Hydraulics consist of three applications, Presmod, Hydraulics and Frictionmaster. Each of these applications is made to perform specific tasks to one or several parts of the drilling operation.

In this project, the Presmod application is the one used for the simulations. Before the specific abilities of this application are described, an explanation as to why this software was chosen is advantageous as a justification to our choice. The Drillbench® software have a good reputation in the industry. It is used by several major companies, with satisfying results. The following quotes are feedback of customer experience, taken from SPT Group (2012).

> *"We have been using Drillbench® Presmod and Kick successfully for well planning and follow-up. In addition, it has been used for crew training purposes on HPHT wells in the UK sector."* ***BP, Aberdeen***
>
> *"The Drillbench® Presmod dynamic hydraulics simulation program was successfully used on the Marlin A-5 well: The program produced accurate downhole temperature and density profiles. The accuracy of the predictions was confirmed by downhole PWD measurements."* ***Baker Hughes Inteq, USA***
>
> *"Both Drillbench® Presmod and Kick have been very useful for decision making in two difficult HPHT wells and have contributed to us reaching the planned targets."* ***ConocoPhilips, Scandinavian Division***

As can be seen, the software has been used in a variety of situations, and by several major companies. Many companies use the software on an everyday basis. The software is continuously improved, and was developed based on more than 15 years of drilling research.

The Drillbench® software was chosen based on its spread in the industry, its reputation, and the availability for usage in this project. It provides the features desired for comparisons purposes, and the visualization options give the required possibilities.

Drillbench® presmod is as mentioned the chosen application. In this part of the software, it is possible to accurately model pressures (ECD and ESD) and temperature profiles for deepwater wells, high pressure high temperature (HPHT) wells, or other wells with narrow margins between pore and fracture pressure, such as ERD wells and wells in depleted reservoirs. This application make it possible to build an imaginary well based on real input parameters, and by selecting the wanted input parameters according to the well to be modeled, simulations of various drilling operations can be carried out.

It is possible to select which fluid systems should be used, the maximum and minimum circulation rates can be chosen, maximum tripping velocities can be set, and from this several operational procedures within pressure limitations can be developed. For this project, the possibility of selecting drillpipe rotation speeds, fluid circulation rates, rheology models and the eccentricity of the pipe, along with the batch simulation feature – choosing which operation should be performed, and for how long–make the Presmod application suitable for comparison purposes.

Several simulations can be run simultaneously, and the graphical presentation of the simulation results can easily be customized. The software can both import and export data from other sources, so it is easy to compare results from for instance a PWD-operation with a simulation, both within the software, and with an external software package, such as Excel.

4.2: Simulation Base Case Data Set

As the field studies presented in chapter 2 suggests, an increase in pressure losses is expected from drillpipe rotation. In this part, a simulation will be performed in Drillbench®, to see whether the software lead to a similar result. To perform a simulation in this software, several

input parameters are required. An example situation was made based on the studies of Marken et al. (1992). The input parameters that are chosen will be presented in the same classifications found in the Drillbench® layout. The sequence of operations chosen to be executed in the simulations, along with the simulation results, will be given in subchapter 4.3

4.2.1: Formation Parameters

In this part, the input parameters for the formation are determined. The surface temperature has to be specified, and the top, bottom and geothermal gradient for the formation sections are specified. The input values chosen are given in **Fig. 6.** At the Ullrigg facility, there is an air gap of 8.75m, and the formation depth is 1575m true vertical depth (TVD). The geothermal gradient had to be assumed for the lithology named formation.

Surface temperature

15,00 Celsius

Depth are true vertical depth with reference to RKB

Lithology name	Top TVD (m)	Bottom TVD (m)	Geothermal gradient (C/m)	Thermophysical properties
Air gap	0,00	8,75	0	
Formation	8,75	1575,00	0,026	

Fig. 6—Drillbench® input parameters for formation.

4.2.2: Survey Parameters

The survey parameters explain the trajectory of the well. Input parameters chosen are presented in **Fig. 7.** From the parameters entered, other input parameters are calculated by the software. The trajectory is specified with values for measured depth, and the corresponding inclination and azimuth. All these input values were found at IRIS (2012).

	Measured depth (m)	Inclination (deg)	Azimuth (deg)	Vertical depth (m)	North (m)	East (m)	Horizontal displacement (m)	Dogleg severity (deg/30 m)
1	0,0	0,0	0,0	0,0	0,00	0,00	0,00	0,00
2	50,0	0,9	-29,7	50,0	0,341	-0,195	0,393	0,54
3	100,0	0,4	-95,1	100,0	0,667	-0,563	0,873	0,49
4	150,0	0,7	142,5	150,0	0,409	-0,551	0,686	0,58
5	200,0	0,9	58,2	200,0	0,373	-0,031	0,375	0,65
6	250,0	0,6	173,2	250,0	0,32	0,334	0,463	0,77
7	300,0	1,3	143,6	300,0	-0,396	0,701	0,805	0,50
8	350,0	6,6	155,6	349,8	-3,472	2,226	4,124	3,20
9	400,0	11,2	143,7	399,2	-10,006	6,29	11,819	2,96
10	450,0	12,7	145,2	448,1	-18,433	12,302	22,161	0,92
11	500,0	12,0	150,8	497,0	-27,484	17,975	32,84	0,83
12	550,0	12,5	154,7	545,9	-36,913	22,823	43,399	0,58
13	600,0	12,2	158,4	594,7	-46,718	27,08	53,999	0,51
14	650,0	13,1	159,0	643,5	-56,92	31,056	64,841	0,55
15	700,0	14,6	153,9	692,0	-67,87	35,859	76,761	1,16
16	750,0	16,2	152,2	740,2	-79,70	41,885	90,036	1,00
17	800,0	16,4	146,1	788,2	-91,729	49,076	104,032	1,03
18	850,0	20,7	138,2	835,6	-104,183	58,909	119,684	2,98
19	900,0	24,6	129,8	881,8	-117,441	72,803	138,176	3,03
20	950,0	27,8	123,2	926,6	-130,493	90,564	158,84	2,59
21	1000,0	31,0	119,2	970,2	-143,164	111,567	181,503	2,25
22	1050,0	32,8	115,6	1012,7	-155,299	135,024	205,79	1,57
23	1100,0	36,5	113,7	1053,8	-167,133	160,864	231,971	2,31
24	1150,0	38,5	109,1	1093,5	-178,206	189,195	259,907	2,06
25	1200,0	40,3	106,5	1132,1	-187,892	219,409	288,866	1,47
26	1250,0	43,0	104,0	1169,4	-196,611	251,465	319,203	1,90
27	1300,0	46,2	104,0	1205,0	-205,104	285,525	351,557	1,92
28	1350,0	50,5	100,6	1238,3	-213,022	322,018	386,101	3,00
29	1400,0	52,3	102,4	1269,5	-220,82	360,303	422,587	1,37
30	1450,0	55,1	100,5	1299,1	-228,806	399,793	460,637	1,91
31	1500,0	58,6	100,2	1326,4	-236,323	440,968	500,301	2,11
32	1550,0	61,8	90,6	1351,3	-240,341	484,088	540,467	5,35
33	1600,0	61,9	88,8	1374,9	-240,11	528,171	580,187	0,95
34	1650,0	63,4	88,4	1397,9	-239,024	572,567	620,456	0,92
35	1700,0	60,1	91,7	1421,5	-239,043	616,596	661,311	2,64
36	1750,0	57,8	93,5	1447,3	-240,977	659,383	702,037	1,66
37	1800,0	57,6	98,9	1474,0	-245,537	701,375	743,112	2,74
38	1850,0	58,2	102,7	1500,6	-253,476	742,968	785,016	1,96
39	1900,0	59,9	105,8	1526,3	-264,039	784,517	827,758	1,89
40	1950,0	60,8	110,5	1551,1	-277,576	825,788	871,192	2,51
41	2000,0	61,3	116,6	1575,3	-295,051	865,866	914,756	3,22

Fig. 7—Drillbench® input parameters for survey.

4.2.3: Pore Pressure and Fracture Pressure Parameters

In order for the software to calculate the mud window, values for pore pressure and fracture pressure have to be specified. For both pore pressure and fracture pressure, the pressure gradient or pressure have to be given for a specified depth. If pressure gradient is chosen, the software will calculate the given pressure, and vice versa. However, this section is not important for the simulation in this project, and will for that reason be omitted.

4.2.4: Wellbore Geometry Parameters

Wellbore geometry parameters include riser and casing specifications. The chosen input values are presented in **Fig. 8.** As can be seen, lengths and diameters are the main parameters chosen for the different sections. For the casing strings, it is also necessary to choose hanger depths and setting depths, along with a value for the top of the cement, and what fluid is above this. For all casing strings, water is chosen as the fluid above the cement.

Riser

Name	Length (m)	Inner diameter (cm)	Outer diameter (cm)	Thermophysical properties

Casing / Liner Depths are measured depth with reference to RKB

Name	Hanger depth (m)	Setting depth (m)	Inner diameter (cm)	Outer diameter (cm)	Hole diameter (cm)	Top of cement (m)	Material above cement	Thermophysical properties
10 3/4" L/N80 45.5 lbs/ft	0,0	229,0	25,3	27,3	44,5	0,00	Default	
9 5/8" L/N80 47.0 lbs/ft	0,0	1575,0	22	24,5	31,8	0,00	Default	
13 3/8" L/N80 72.0 lbs/ft	0,0	1330,0	31,4	34	44,5	0,00	Default	

Fig. 8—Drillbench® input parameters for wellbore geometry.

4.2.5: String Input Parameters

The chosen values for the input parameters of the string are given in **Fig. 9.** Lengths and diameters are specified for each pipe component. This is also where the parameters for the drill bit has to be chosen. The software has the possibility of choosing from a list of components with pre-entered values for some of the parameters. It is also possible to add components to the list for future simulations.

Average stand length 30,00 m ☐ Use tool joints

Components are specified from bottom to top

Component	Type	Section length (m)	Inner diameter (cm)	Outer diameter (cm)	Distance from bottom (m)	Thermophysical properties	Properties
DC 6 1/2" Nc 46-65 (4 IF)	DrillCollar	210,0	8,890	16,510	210,0		
dp 5" E75 19.50 lb/ft	Drillpipe	1385,0	10,860	12,700	1595,0		

Bit data
Bit: Bit 8 1/2 pdc
Bit / Open hole diameter: 21,6 cm
Area definition method: Total flow area
Total nozzle area: 0,00045 m2

Fig. 9—Drillbench® input parameters for string components.

4.2.6: Mud Input Parameters

This is perhaps the most important section regarding this project. Here, the input values for the drilling fluid properties have to be chosen, and these may directly affect the outcome when looking at pipe rotational effects on ECD. In **Fig. 10,** the input values for fluid component densities are given. This is also where the PVT model and rheology model is selected. In this example, the rheology model selected is the Power law. As can be seen, the selected model is represented by Fann readings. Three different OBM were used in the study by Marken et al. (1992), and this is also chosen for this example. The input parameters of Fig. 10 will be the same for all three fluids, except for the density, which were 1300 kg/m^3, 1500 kg/m^3 and 1700 kg/m^3 respectively. The Fann readings for these three fluids are given in **Figs. 11 through 13.**

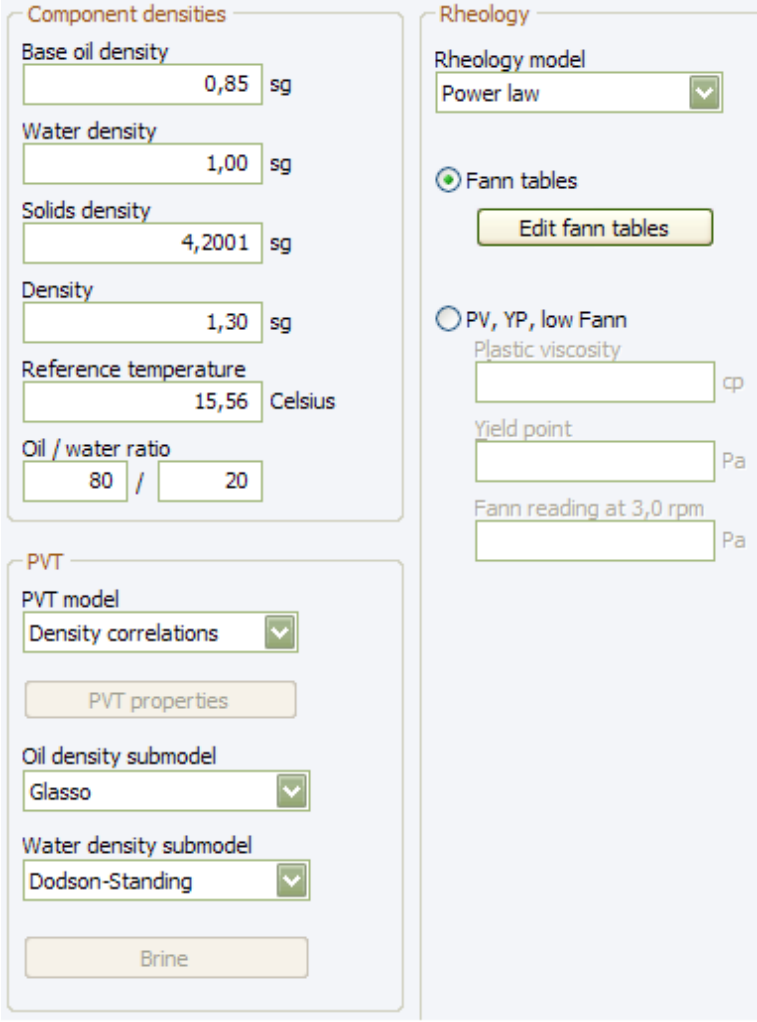

Fig. 10—Drillbench® input parameters for mud properties.

Temperature (Celsius)	Pressure (bar)	600 RPM (Pa)	300 RPM (Pa)	200 RPM (Pa)	100 RPM (Pa)	60 RPM (Pa)	30 RPM (Pa)	6 RPM (Pa)	3 RPM (Pa)
20,00	1	112	65						

Fig. 11—Fann readings used as rheology model input with fluid density of 1300 kg/m^3.

Temperature (Celsius)	Pressure (bar)	600 RPM (Pa)	300 RPM (Pa)	200 RPM (Pa)	100 RPM (Pa)	60 RPM (Pa)	30 RPM (Pa)	6 RPM (Pa)	3 RPM (Pa)
20,00	1	148	86						

Fig. 12—Fann reading used as rheology model input with fluid density of 1500 kg/m^3

Temperature (Celsius)	Pressure (bar)	600 RPM (Pa)	300 RPM (Pa)	200 RPM (Pa)	100 RPM (Pa)	60 RPM (Pa)	30 RPM (Pa)	6 RPM (Pa)	3 RPM (Pa)
20,00	1	200	116						

Fig. 13—Fann reading used as rheology model input with fluid density of 1700 kg/m^3

4.2.7: Temperature Input Parameters

Values for temperature parameters were chosen to be found from models within the Drillbench® software. The surface temperature model on the platform was chosen to be calculated from a heat loss constant of 40, and an initial pit temperature of 298.15 °K. For other sections of the well, a dynamic temperature model was chosen to be calculated from the initial mud temperature by usage of the geothermal gradient.

4.3: Results of Drillbench® Simulations

There is no description of the equations used to calculate the contribution of pipe rotation to ECD in Drillbench®. However, it is possible to get a plot of the ECD changes versus rotation speed. To make the Drillbench® example as close as possible to the field study it is based on, this plot is made for all three mud weights. The sequence of the operations it simulates is also found from the study of Marken et al. (1992).

For the 1300 kg/m^3 mud, the flow rate is 0.030 m^3/s, and this rate is kept constant. Before a simulation is possible, a value for torque had to be chosen, and this was set to 10000Nm. The rate of penetration was kept at 0, and the inlet temperature was chosen to be 15.56°C. A time of 2 minutes was chosen for each rotation velocity, and the rotation velocities were chosen to start on 0 RPM, and have a 5 RPM increment until it reached 600 RPM. The total time of the "operation" would then be 242 minutes. **Fig. 14** shows the ECD variation versus time.

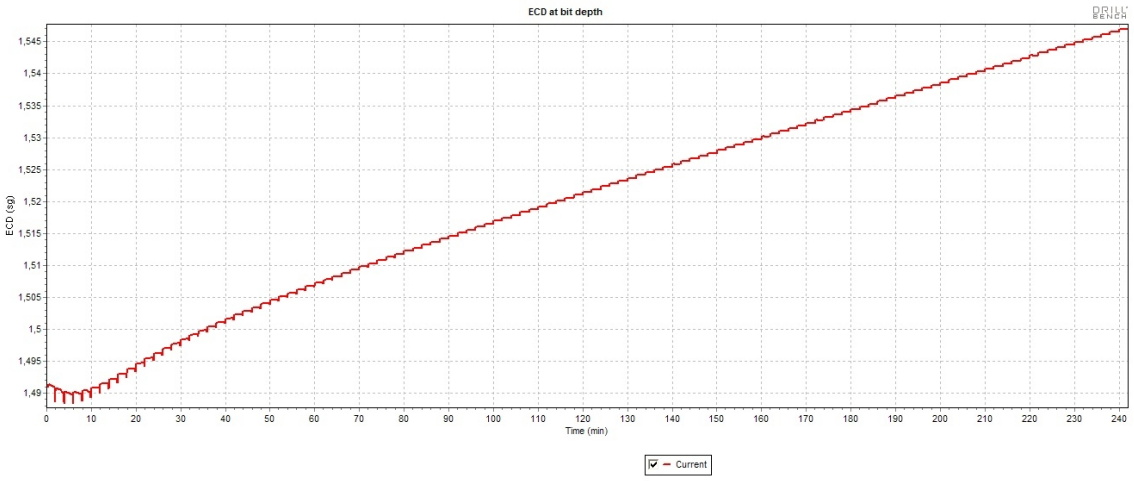

Fig. 14—Resulting plot of ECD versus time for 1300 kg/m^3 drilling fluid

When simulation was performed by use of the 1500 kg/m^3 drilling fluid, the same input parameters was chosen, the flow rate was chosen to be 0.030 m^3/s, the ROP was kept at 0, initial torque was set at 10000Nm, and inlet temperature was 15.56°C. **Fig. 15** shows the resulting plot of ECD versus time, with the same sequence of operations chosen as for the previous case. In **Fig. 16,** the ECD versus time is plotted for the 1700 kg/m^3 mud. All the parameters are the same for this case as for the two other cases, but with a mud weight of 1700 kg/m^3, and the Fann-readings from this fluid.

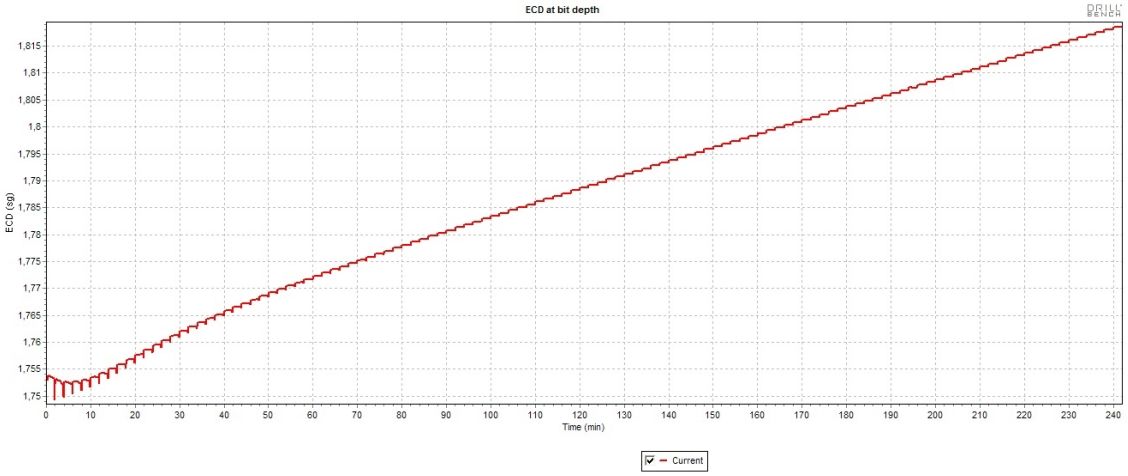

Fig. 15—Resulting plot of ECD versus time for 1500 kg/m^3 drilling fluid

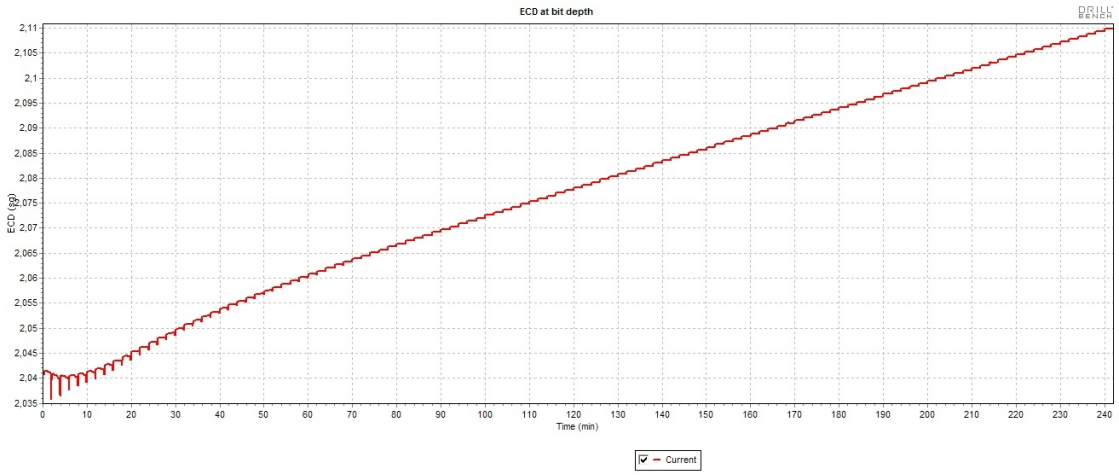

Fig. 16—Resulting plot of ECD versus time for 1700 kg/m^3 drilling fluid

These graphs provide the values needed for comparison with the empirical equation on the form $\Delta P_{\omega \neq 0}/\Delta P_{\omega=0}$ vs. RPM developed in chapter 5. How this is done will be presented in this chapter.

Chapter 5: Development of Own Models Through Regression Analysis

This part of the report is where the empirical equations will be derived. The chapter will also present how the data sets were generated, how the data were prepared to do the regression analysis, general curve fittings theory will be given, and the accuracy of the equations will be tested by comparison to simulation results, calculations by usage of the PLR-equation from chapter 3, and an independent field study.

5.1: Data Sets Generation

One of the main challenges with this project was to generate the data sets. There are not much public data, and the data sets that are available have to be organized to be used in the regression analysis. This fact lead to two weaknesses with the equations, they are made from few data points, and there are no possibilities for gathering more information regarding the data sets to improve the accuracy of these data points.

To make the regression analysis as precise as possible, the data sets were collected and sorted in groups. One of the groups was data on the form *pressure losses with rotation / pressure losses without rotation* ($\Delta P_{\omega\neq 0}/\Delta P_{\omega=0}$) vs. *revolutions per minute (RPM)*. In the study by Delwiche et al. (1992), pressure data versus rotation rate was studied by Total and DB Stratabit Ltd (DBS). This data was collected for three different situations of a slim-hole well. The data in this study was presented on the form ωR/U (dimensionless ratio between rod tangential velocity and mud axial averaged velocity). Here, ω [rad/s] is the angular rod rotation speed, R [m] is the rod radius, and U [m/s] is the axial averaged velocity. When data was collected from this study, this dimensionless number had to be converted to RPM. Data was available for three different situations.

The first situation, called 578P1172, represents data from a well drilled to a depth of 1180 meters, with a 6.625-in. casing set at 937 meters, and with an openhole diameter of 5.875 in. for the remaining interval. The drillpipe used had an outer diameter of 5 in. The data was collected from **Fig. 22** replicated in Appendix A, and the result is listed in **Table 1.** The rotation speed was converted from ωR/U to RPM with $R=OD_{pipe}/2=0.0635$ m, and U=0.5 m/s.

Table 1—Pressure losses vs. RPM data from 578P1172. DBS on the left side, Total on the right side.

$\Delta P_{\omega\neq0}/\Delta P_{\omega=0}$	RPM
1.137	58.4
1.218	74.5
1.209	84.6
1.257	96.0
1.230	109.4
1.237	109.5
1.287	129.3
1.310	141.7
1.325	141.7
1.406	173.2
1.406	211.5
1.615	261.1

$\Delta P_{\omega\neq0}/\Delta P_{\omega=0}$	RPM
1.355	58.4
1.513	74.5
1.272	84.6
1.436	96.0
1.331	109.4
1.558	109.5
1.699	129.3
1.454	141.7
1.510	141.7
1.630	173.2
1.534	211.5
1.842	261.1

The second situation, called 425P1210, contains data from the same well, only now drilled to a depth of 1214 meters, with a 5-in. casing set at this depth. The drillpipe used had an outer diameter of 3.7 in. The data was read from **Fig. 25** replicated in Appendix A, and the resulting data points are here listed in **Table 2.** The rotation speed was converted to RPM by use of $R=OD_{pipe}/2=0.047$ m, and U=0.5 m/s.

Table 2—Pressure losses vs. RPM data from 425P1210. DBS data to the left, Total to the right.

$\Delta P_{\omega\neq0}/\Delta P_{\omega=0}$	RPM
1.057	30.015
1.043	33.478
1.086	43.868
1.100	58.875
1.100	58.875
1.129	70.419
1.186	87.735
1.186	87.735
1.186	87.735
1.243	105.051
1.207	117.750
1.264	117.750
1.300	132.757
1.250	140.838
1.250	146.610
1.286	177.779
1.300	177.779
1.343	177.779
1.500	177.779
1.350	220.493
1.393	236.654
1.529	265.515
1.500	295.529
1.621	354.405
2.429	354.635
1.786	437.522
2.200	525.257

$\Delta P_{\omega\neq0}/\Delta P_{\omega=0}$	RPM
1.071	30.015
1.029	33.478
1.043	43.868
1.050	58.875
1.179	58.875
1.179	70.419
1.121	87.735
1.214	87.735
1.271	87.735
1.250	105.051
1.264	117.750
1.479	117.750
1.357	132.757
1.443	140.838
1.336	146.610
0.979	177.779
1.500	177.779
1.650	177.779
1.707	177.779
1.600	220.493
1.871	236.654
2.029	265.515
2.014	295.529
1.221	354.405
2.286	354.635
2.229	437.522
1.386	525.257

The third situation is called 425P2078. Here, a well was drilled to a depth of 2078 meters. A 5-in. casing string was set at a depth of 1214 meters, and the open hole section down to 2078 meters had a diameter of 4¼ in. The outer pipe diameter was 3.7 in. The data was read from **Fig. 28** replicated in Appendix A, and the resulting data points are listed in **Table 3.** The rotation speed was converted to RPM by use of $R=OD_{pipe}/2=0.047$ m, and U=0.5 m/s.

Table 3—Pressure losses vs. RPM data from well 425P2078. DBS to the left, Total to the right.

$\Delta P_{\omega\neq0}/\Delta P_{\omega=0}$	RPM
2.067	181.627
2.117	212.412
2.221	261.667
2.263	277.059
2.358	323.235
2.346	332.471
2.492	395.579
2.571	463.304
2.675	507.941
2.825	711.118

$\Delta P_{\omega\neq0}/\Delta P_{\omega=0}$	RPM
2.000	181.627
2.163	212.412
2.150	261.667
2.329	277.059
2.508	323.235
2.142	332.471
2.617	395.579
2.350	463.304
2.592	507.941
2.842	711.118

Haige et al. (2000) presented a study of annular pressure losses in a slimhole well. The well where the measurements were done is called Miao 1-40. In this study, they looked at the effect of drillpipe rotation on annular pressure losses, and presented the results as can be seen in **Fig. 30** of Appendix B. To make this data useful, it had to be converted to the same form as for the previous study presented, *pressure losses with rotation / pressure losses without rotation* ($\Delta P_{\omega\neq0}/\Delta P_{\omega=0}$) vs. *revolutions per minute (RPM)*. This was done simply by dividing the given pressure gradients for the various rotation speeds with the pressure gradient of no rotation. The result for three scenarios are presented in **Table 4,** case 1 contained data collected with a velocity of 0.532 m/s, case 2 with a velocity of 0.802 m/s, and case 3 was for a mud velocity of 1.15 m/s.

Table 4—Pressure losses vs. RPM from Miao 1-40 well. Case 1 to the left, case 2 in the middle, and case 3 to the right.

$\Delta P_{\omega\neq0}/\Delta P_{\omega=0}$	RPM
1.014	30
1.034	70
1.103	110
1.179	150

$\Delta P_{\omega\neq0}/\Delta P_{\omega=0}$	RPM
0.978	30
1.022	70
1.087	110
1.087	150

$\Delta P_{\omega\neq0}/\Delta P_{\omega=0}$	RPM
0.974	30
1.008	70
1.026	110
1.110	150

In a study by Diaz et al. (2004), data from a casing drilling operation collected by MoBPTeCh Alliance from the Baker Hughes Experimental Test Area (BETA) was presented. In this study, the accuracy of several theoretical models for calculating ECD were compared to

measured data. This was done with three different drilling fluids, water, Mud A and Mud B. The results was presented as RPM versus bottomhole pressure (BHP), as can be seen in **Fig. 33 through Fig. 41** of Appendix C. To make the measured data useful for this project, several calculations had to be made. For each of the three drilling fluids, ESD was calculated from its given densities, and the data read from the plots could be made on the form ΔP by subtracting ESD. By comparing ΔP with rotation to ΔP without rotation, the numbers would be on the desired form, $\Delta P_{\omega\neq 0}/\Delta P_{\omega=0}$ vs. *RPM*. For each of the three drilling fluids, three sets of data were measured in the study, with a variation in the pump rate, 0.022 m^3/s, 0.028 m^3/s and 0.035 m^3/s. The data was treated in the same manner as already mentioned for each of these situations, and the result can be seen in **Table 5, Table 6 and Table 7.** Table 5 represent the data measured with water as the drilling fluid, and a density of 998.15 kg/m^3 for each of the three flow rates. The depth of this well section was 86.26 m, with a wellbore diameter of 12.715 in., and an outer casing diameter of 11.75 in.

Table 5—Data of pressure losses vs. RPM collected from BETA. Water as the drilling fluid, Q=0.022 m^3/s to the left, Q=0.028 m^3/s in the middle, and Q=0.035 m^s/s to the right.

$\Delta P_{\omega\neq 0}/\Delta P_{\omega=0}$	RPM
1.265	60
1.088	120
1.941	180

$\Delta P_{\omega\neq 0}/\Delta P_{\omega=0}$	RPM
1.073	60
1.215	120
1.035	180

$\Delta P_{\omega\neq 0}/\Delta P_{\omega=0}$	RPM
1.121	60
1.301	120
1.462	180

Table 6 represent the data measured in the same well, but with Mud A (a bentonite/water mixture) as drilling fluid. The density of the drilling fluid was 1042.49 kg/m^3, the depth was 86.26 m, with a wellbore diameter of 12.715 in., and a casing diameter of 11.75 in.

Table 6—Data of pressure losses versus RPM collected from BETA. Mud A as the drilling fluid, Q=0.022 m^3/s to the left, Q=0.028 m^3/s in the middle, and Q=0.035 m^3/s to the right. No data was found above 120 RPM for Q=0.022 m^3/s.

$\Delta P_{\omega\neq 0}/\Delta P_{\omega=0}$	RPM
1.449	60
1.296	120
xxxx	xxxx

$\Delta P_{\omega\neq 0}/\Delta P_{\omega=0}$	RPM
1.147	60
1.172	120
0.824	180

$\Delta P_{\omega\neq 0}/\Delta P_{\omega=0}$	RPM
0.963	60
1.023	120
0.731	180

Table 7 contains data measured in the same well as previously described, but with Mud B (a bentonite/water mixture) as drilling fluid. As for the previous cases, the depth was 86.26 m, the wellbore diameter was 12.715 in., and the outer casing diameter was 11.75 in. The density of Mud B was found to be 1174.30 kg/m^3.

Table 7—Data of pressure losses versus RPM collected from BETA. Mud B as the drilling fluid, Q=0.022 m^3/s to the left, Q=0.028 m^3/s in the middle, and Q=0.035 m^3/s to the right.

$\Delta P_{\omega\neq0}/\Delta P_{\omega=0}$	RPM
1.335	60
1.646	120
2.508	180

$\Delta P_{\omega\neq0}/\Delta P_{\omega=0}$	RPM
0.920	60
1.196	120
1.437	180

$\Delta P_{\omega\neq0}/\Delta P_{\omega=0}$	RPM
0.921	60
1.036	120
1.251	180

In the study by Hemphill et al. (2007), well data from two tests carried out on the 22/30c-G4 well at the Elgin-Franklin UKCS fields were presented. The data were presented as *measured change in ECD (lbm/gal)* vs. *drillpipe rotation speed (RPM)*, and consequently, the data had to be converted to the form *pressure losses with rotation / pressure losses without rotation* ($\Delta P_{\omega\neq0}/\Delta P_{\omega=0}$) vs. *revolutions per minute (RPM)* to compare them with the other data sets collected. In this study, it was referred to a study by Isambourg et al. (1999) for further details, and this is the source of the parameters used in the conversion process. After the data points for the two tests (Elf 8.75-in A and Elf 8.75-in B) had been found, the values for measured change in ECD (lbm/gal) was converted to measured change in ECD (kg/m^3). The ECD with no pipe rotation was found to be 2233 kg/m^3, while the ESD was found to be 2190 kg/m^3; hence the ECD increase with no rotation was 43 kg/m^3. By dividing the converted data points with this ECD increase, all data was on the required form. The data points on the final form are presented in **Table 8,** and a copy of the original source can be found in **Fig. 43** of Appendix E.

Table 8—Welldata from the 22/30c-G4 well, test Elf 8.75-in A to the left, and Elf 8.75-in B to the right.

$\Delta P_{\omega\neq0}/\Delta P_{\omega=0}$	RPM
0.121	60
0.407	120
0.468	150
0.606	180

$\Delta P_{\omega\neq0}/\Delta P_{\omega=0}$	RPM
0.224	60
0.447	120
0.700	180

For the second type of empirical equations predicting pressure losses caused by drillpipe rotation, it was decided that more consideration had to be given to the well characterizations and the fluid behavior. To do this, the Reynolds number was chosen to be used as the basis of the equations. The data sets were collected on the form $\Delta P_{\omega\neq0}/\Delta P_{\omega=0}$ vs. Reynolds number, and consequently, equations had to be made for several rotation speeds.

After a process of gathering possible data sets, three rotation speeds were found to have a large enough number of data points to do the regression analysis. These rotation speeds were 200 RPM, 300 RPM and 600 RPM. The first data points that could be converted to the

required form were found from the study of Delwiche et al. (1992). In well 578P1172, described in detail earlier in this chapter, measurements of the pressure losses were done at a variety of mud flow rates for a pipe rotation speed of 200 RPM, as seen in **Fig. 23** of Appendix A. This data had to be converted to get it in on the form $\Delta P_{\omega\neq0}/\Delta P_{\omega=0}$ vs. Reynolds number. The pressure loss data was converted to $\Delta P_{\omega\neq0}/\Delta P_{\omega=0}$ data by dividing the pressure loss value at 200 RPM with the value for that of no rotation. To get the mud flow expressed by the Reynolds number, the flow rate had to be converted to mud velocity by dividing it with the flow area of the annulus, and then the Reynolds numbers were calculated with the general equation for Reynolds number:

$$\mathrm{Re} = \frac{\rho v d}{\mu_{eff}} \tag{5.1}$$

The rheology model that best fitted this measurement was the Power law; hence the values for μ_{eff} were calculated from the equation representing effective viscosity in annulus for the Power law model:

$$\mu_{eff} = \left(\frac{12\overline{v}}{d_h} \cdot \frac{2n+1}{3n} \right)^n \cdot \frac{K d_h}{12\overline{v}} \tag{5.2}$$

All input data for the calculations can be found in **Table 27** of Appendix H, along with a copy of the original source for the data sets. The final data points are presented in **Table 9.**

Table 9—Welldata from 578P1172 on the form $\Delta P_{\omega\neq0}/\Delta P_{\omega=0}$ vs. Reynolds number, RPM=200

$\Delta P_{\omega\neq0}/\Delta P_{\omega=0}$	Re
1.475	184
1.389	303
1.479	432
1.353	569

In the same study, data points were collected from well 425P1210 for 200 RPM (see **Fig. 26** of Appendix A). The same conversions had to be made on these data points, and the input values for the calculations can be found in **Table 28** of Appendix H. The final data points are presented in **Table 10.**

Table 10—Welldata from 425P1210 on the form $\Delta P_{\omega\neq0}/\Delta P_{\omega=0}$ vs. Reynolds number, RPM=200

$\Delta P_{\omega\neq0}/\Delta P_{\omega=0}$	Re
1.286	10
1.800	23
1.460	39
1.247	56
1.174	74
1.059	93

Bode et al. (1989), presented a study of a test well called SHADS #7. This well was drilled down to 609.6 m, with a 5-in. casing and a 3.7-in. drillstring. Measurements of the annular pressure loss with rotation to that without rotation was plotted against the Reynolds number for a rotation speed of 200 RPM, as can be seen in **Fig. 42** of Appendix D. The resulting data set can be seen in **Table 11.**

Table 11—Welldata from SHADS #7 testwell on the form $\Delta P_{\omega\neq0}/\Delta P_{\omega=0}$ vs. Reynolds number, 200 RPM rotation speed.

$\Delta P_{\omega\neq0}/\Delta P_{\omega=0}$	Re
1.673	426
1.684	721
2.220	971
1.724	1103
1.704	1471
1.857	1574
1.551	2217
1.796	2348
1.404	2913
1.531	3382
1.319	3632
1.245	4391
1.394	4478
1.298	5632
1.255	6841

In the study by Delwiche et al. (1992), data from well 425P2078 was presented in the same manner as for the two other wells from this study (see **Fig. 29** of Appendix A), and the same conversions had to be made on this data set to make it useful. The input for the calculations that was performed can be found in **Table 29** of Appendix H, and a summary of the data points are presented in **Table 12.** The rotation speed in this measurement was 300 RPM.

Table 12—Welldata from 425P2078 on the form $\Delta P_{\omega\neq0}/\Delta P_{\omega=0}$ vs. Reynolds number, rotation speed was 300 RPM.

$\Delta P_{\omega\neq0}/\Delta P_{\omega=0}$	Re
2.143	57
1.917	86
2.042	117
1.967	149
1.939	183

McCann et al. (1993) studied how ECD was affected by drillpipe rotation in a slimhole test well called SHDT.1. They measured the ECD increase at different flow rates for a rotation rate of 300 RPM, presented in **Fig. 44** of Appendix F. This data set had to be converted to get it on the required form. The Reynolds numbers were calculated for several flow rates, by use of the general form of Reynolds number, and the effective viscosity was calculated from the

Newtonian model because water was used as drilling fluid. All calculation input can be found in **Table 30** of Appendix H, and the resulting data set is given in **Table 13.**

Table 13—Welldata from SHDT.1 testwell on the form $\Delta P_{\omega\neq0}/\Delta P_{\omega=0}$ vs. Reynolds number, pipe rotation was 300 RPM

$\Delta P_{\omega\neq0}/\Delta P_{\omega=0}$	Re
1.818	298
1.588	398
1.565	497
1.533	597
1.400	696
1.420	796
1.317	895
1.316	995
1.289	1094
1.260	1194
1.233	1293

In the same study by McCann et al. (1993), they measured the ECD increase for different flow rates with a rotation speed of 600 RPM in the same well. These measurements were presented in the same way as with the 300 RPM rotation speed (see Fig. 44 of Appendix F), and consequently the same conversions had to be made. The input values from these calculations can be found in Table 30 of Appendix H, and the resulting data set is given in **Table 14.**

Table 14—Welldata from SHDT.1 testwell on the form $\Delta P_{\omega\neq0}/\Delta P_{\omega=0}$ vs. Reynolds number, rotation speed was 600 RPM

$\Delta P_{\omega\neq0}/\Delta P_{\omega=0}$	Re
2.545	298
2.118	398
2.000	497
1.900	597
1.750	696
1.680	796
1.587	895
1.487	995
1.456	1094
1.423	1194
1.392	1293

In the study by Bode et al. (1989) earlier described, it was also done measurements of the annular pressure losses with rotation over the annular pressure losses without rotation for a rotation speed of 600 RPM on the SHADS #7 test well, as seen in Fig. 42 of Appendix D. All well parameters were the same for this test as with the one using a rotation speed of 200 RPM. A presentation of the final data set can be found in **Table 15.**

Table 15—Welldata from SHADS #7 testwell on the form $\Delta P_{\omega\neq0}/\Delta P_{\omega=0}$ vs. Reynolds number, rotation speed is 600 RPM

$\Delta P_{\omega\neq0}/\Delta P_{\omega=0}$	Re
1.837	426
2.060	721
2.860	971
2.170	1103
2.130	1471
2.510	1574
2.110	2217
2.590	2348
1.867	2913
2.140	3382
1.745	3632
1.633	4391
1.929	4478
1.857	5632
1.653	6841

5.2: Resulting Regressed Equations

From the data sets presented in the previous subchapter, empirical equations describing the effect of pipe rotation on the annular pressure drop and ECD was developed. The first equation was found with the data sets on the form $\Delta P_{\omega\neq0}/\Delta P_{\omega=0}$ vs. RPM. All the data was gathered in one Excel sheet, and plotted against each other. From this plot, a best-fit line was selected, along with the equation describing this line, and the R^2-value. The R^2-value is a statistical value describing how well the regressed line approximates to the real data points. It ranges from 0 to 1, and the closer it is to 1, the better the approximation. As can be seen in the resulting graph presented in **Fig. 17**, the R^2 value is 0.5921. The empirical equation found was:

$$y = -2E-06x^2 + 0,0043x + 0,7831 \tag{5.3}$$

In this equation, y represents $\Delta P_{\omega\neq0}/\Delta P_{\omega=0}$, and x represents RPM. In the next part of this subchapter, the accuracy of this equation will be tested against Drillbench® simulations, a field study that was not used in the regression analysis, and the equation presented in chapter 3, called the PLR-equation.

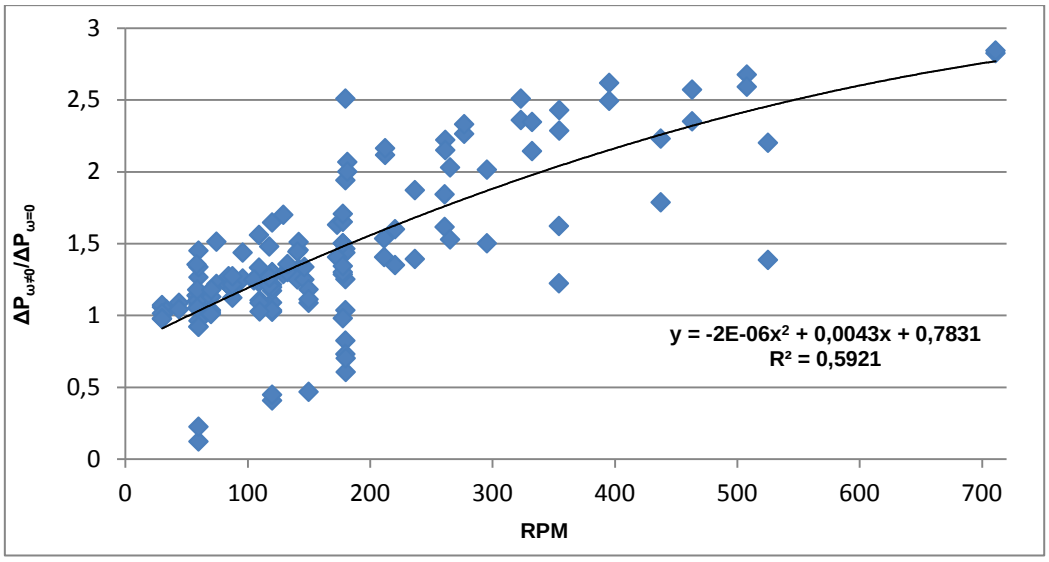

Fig. 17—Plot of gathered data on the form $\Delta P_{\omega\neq0}/\Delta P_{\omega=0}$ vs. RPM, with the resulting empirical equation from the regressed line.

The second type of equations developed from the regression analysis was found by use of the data points on the form $\Delta P_{\omega\neq0}/\Delta P_{\omega=0}$ vs. Reynolds number. Three equations were made, representing rotation speeds of 200 RPM, 300 RPM and 600 RPM. As with the previous equation, the value for R^2 is a description of how well the equations predict values based on real data points. The plot and equation with a rotation speed of 200 RPM can be seen in **Fig. 18,** while the plot and equation for a rotation speed of 300 RPM is given in **Fig. 19. Fig. 20** contains the plot of the data sets for 600 RPM.

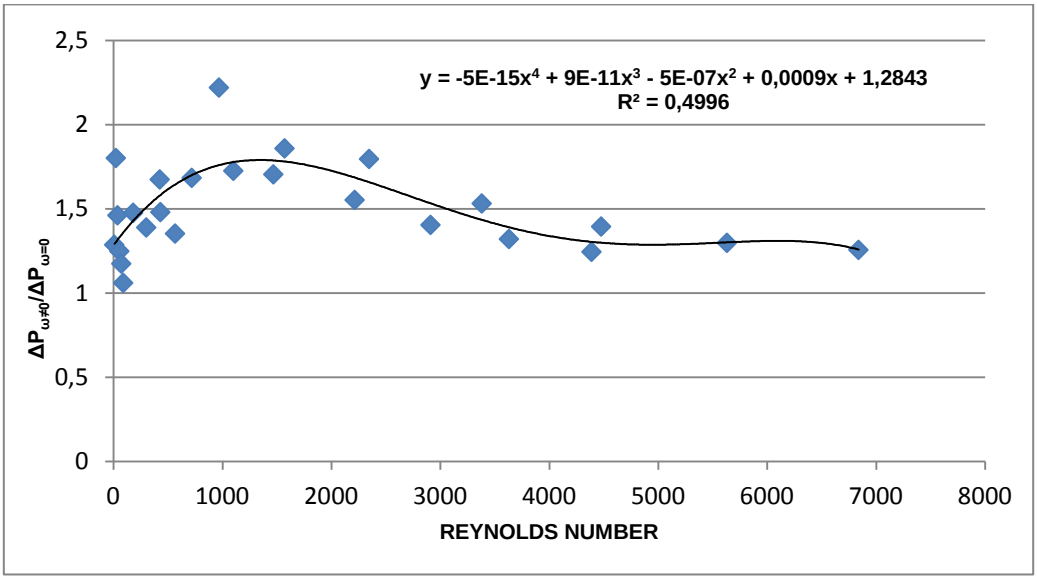

Fig. 18—Plot of gathered data on the form $\Delta P_{\omega\neq0}/\Delta P_{\omega=0}$ vs. Re, with the resulting empirical equation from the regressed line of a 200 RPM rotation speed.

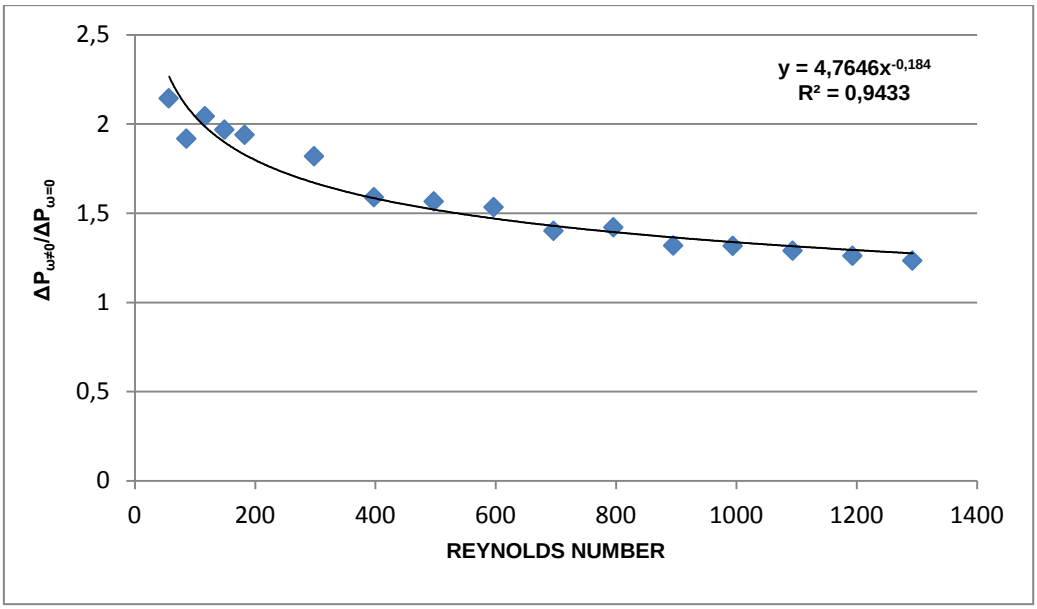

Fig. 19—Plot of gathered data on the form $\Delta P_{\omega\neq0}/\Delta P_{\omega=0}$ vs. Re, with the resulting empirical equation from the regressed line of a 300 RPM rotation speed.

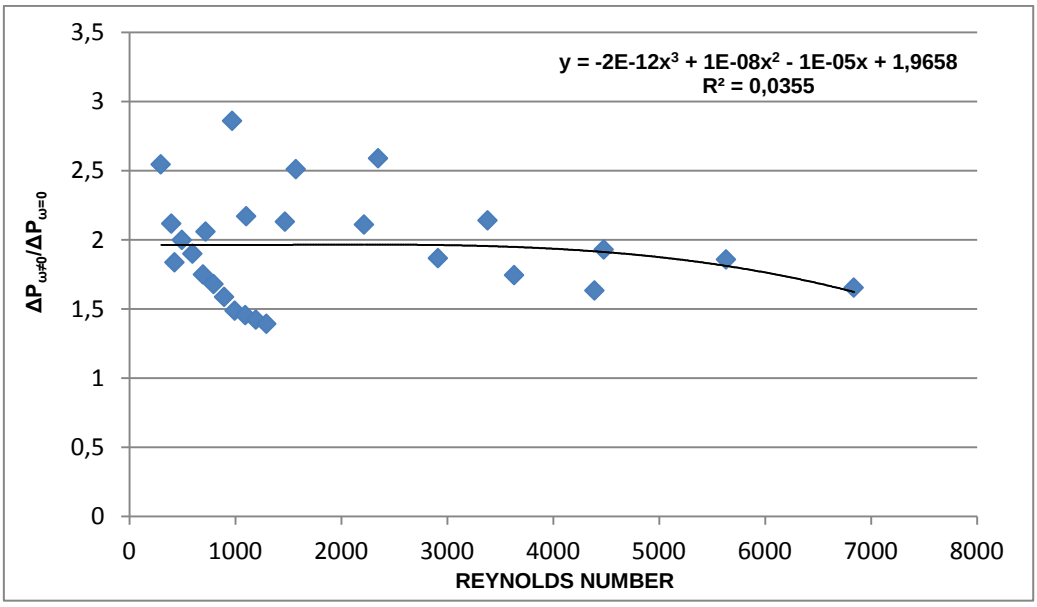

Fig. 20—Plot of gathered data on the form $\Delta P_{\omega\neq0}/\Delta P_{\omega=0}$ vs. Re, with the resulting empirical equation from the regressed line of a 600 RPM rotation speed.

As can be seen in Fig. 18, the empirical equation for $\Delta P_{\omega\neq0}/\Delta P_{\omega=0}$ versus Reynolds number for a rotation speed of 200 RPM is:

$$y = -5\cdot10^{-15}x^4 + 9\cdot10^{-11}x^3 - 5\cdot10^{-7}x^2 + 0,0009x + 1,2843 \qquad (5.4)$$

The variable y represents $\Delta P_{\omega\neq0}/\Delta P_{\omega=0}$, and x represents the Reynolds number. For this equation, the R^2-value is 0.4996. With this equation, it is possible to predict the additional pressure losses caused by rotation at a speed of 200 RPM, at given Reynolds numbers. The same equation for a rotation speed of 300 RPM is given by:

$$y = 4,7646 \cdot x^{-0,184} \quad (5.5)$$

The variables are the same as for the previous equation. R^2=0.9433 for this equation, meaning that it is close to the real data points. For the 600 RPM rotation speed, the equation was found to be:

$$y = -2 \cdot 10^{-12} x^3 + 1 \cdot 10^{-8} x^2 - 1 \cdot 10^{-5} x + 1,9658 \quad (5.6)$$

The R^2-value is 0.0355, and the regressed line is thereby not an accurate prediction of the data points. The presented equations will be tested against an existing semi-empirical equation, and against real drilling data from a field study later in this chapter.

5.3: Results

As was seen in Fig. 17, the resulting regressed equation from the data sets on the form $\Delta P_{\omega \neq 0}/\Delta P_{\omega=0}$ vs. RPM predict a substantial pressure loss with increasing rotation speeds. This is as expected from the data sets gathered, because much of the data used originate from slimhole drilling, in which rotation of the drillpipe can give as much as 90% of the total annular pressure losses. However, because larger pressure losses are expected for slimhole drilling than for conventional drilling, it is expected that this equation will predict a value above the actual pressure loss ratio. By comparing with the Drillbench® simulation based on a field study, and the predicted values from the semi-empirical equation presented in chapter 3, it can be seen whether this expectation is fulfilled.

The three regressed equations on the form $\Delta P_{\omega \neq 0}/\Delta P_{\omega=0}$ vs. Reynolds number do not have the same shape, but they have some similarities. The pressure loss with rotation over that without rotation is decreasing with an increasing Reynolds number. This is as expected because the mud flow would not be affected as much by pipe rotation for a turbulent flow as for a laminar flow. These equations will also be compared to Drillbench® simulations and the PLR-equation from chapter 4, but there is not enough field data to test the accuracy of the equations by comparing with a dataset not used in the creation of the equations.

5.3.1: Comparison With Drillbench® Simulations

In this section, the regressed equations will be compared to the results of the Drillbench® simulations done in chapter 4. The first equation to be compared, is the one derived from the data sets on the form $\Delta P_{\omega \neq 0}/\Delta P_{\omega=0}$ vs. RPM. This is done by choosing to look at specific rotation speeds, and compare the calculated values of the empirical equation with the values

obtained in Drillbench® for these rotation speeds. The rotation speeds chosen to be looked at, are 60 RPM, 120 RPM, 150 RPM, 200 RPM, 400 RPM and 600 RPM. From the figures in chapter 4 representing the simulation results, it was seen that the plot was ECD versus time. The time can easily be converted to RPM because a constant time of two minutes was chosen for every 5 RPM increase. In the Drillbench® software, it is possible to track the values of a graph, and this was done to find the corresponding ECD value for the 6 rotation speeds. Because ECD is not the value to be compared, these numbers had to be converted to the form $\Delta P_{\omega\neq0}/\Delta P_{\omega=0}$. This was done by dividing the sum of the ECD value read from the graph and ESD (the mud weight in SG), with the sum of ECD with no rotation and the ESD:

$$\Delta P_{\omega\neq0} / \Delta P_{\omega=0} = \frac{(ECD_{read} - ESD)}{(ECD_{0\,RPM} - ESD)} \tag{5.7}$$

These values were calculated by use of the three different mud weights. The comparison with the approximations from the empirical equation for the 1300 kg/m^3 mud is shown in **Table 16;** the comparison with the 1500 kg/m^3 is shown in **Table 17,** and with the 1700 kg/m^3 mud in **Table 18.**

Table 16—Comparison of results from simulation and empirical equation, mud weight 1300 kg/m^3

RPM	$\Delta P_{\omega\neq0}/\Delta P_{\omega=0}$ from Drillbench®	$\Delta P_{\omega\neq0}/\Delta P_{\omega=0}$ vs. RPM-equation	Difference [%]
60	1.0244	0.9931	−3.06 %
120	1.0634	1.1931	12.19 %
150	1.0801	1.3831	28.05 %
200	1.1061	1.5631	41.32 %
400	1.1992	2.1831	82.05 %
600	1.2845	2.6431	105.78 %

Table 17—Comparison of results from simulation and empirical equation, mud weight 1500 kg/m^3

RPM	$\Delta P_{\omega\neq0}/\Delta P_{\omega=0}$ from Drillbench®	$\Delta P_{\omega\neq0}/\Delta P_{\omega=0}$ vs. RPM-equation	Difference [%]
60	1.0208	0.9931	−2.71 %
120	1.0553	1.1931	13.06 %
150	1.0698	1.3831	29.29 %
200	1.0921	1.5631	43.13 %
400	1.1733	2.1831	86.07 %
600	1.2489	2.6431	111.63 %

Table 18—Comparison of results from simulation and empirical equation, mud weight 1700 kg/m^3

RPM	$\Delta P_{\omega\neq0}/\Delta P_{\omega=0}$ from Drillbench®	$\Delta P_{\omega\neq0}/\Delta P_{\omega=0}$ vs. RPM-equation	Difference [%]
60	1.0093	0.9931	−1.61 %
120	1.0420	1.1931	14.50 %
150	1.0533	1.3831	31.31 %
200	1.0708	1.5631	45.97 %
400	1.1349	2.1831	92.35 %
600	1.1947	2.6431	121.24 %

As can be seen from these tables, the difference between the predicted result by use of the $\Delta P_{\omega\neq0}/\Delta P_{\omega=0}$ vs. RPM-equation and the Drillbench® simulation is increasing with increasing rotation rate for all three mud weights. Either the equation is predicting a too large pressure loss for high rotation speeds, or the software is predicting too low values. By comparing with the PLR-equation and a field study in the next subchapter, an answer to this will be found.

To test the equations on the form $\Delta P_{\omega\neq0}/\Delta P_{\omega=0}$ versus Reynolds number, simulations in Drillbench® had to be made based on the Reynolds number. This is not a parameter that can be chosen, so it had to be found by modifying the input parameters according to equation (5.1). Two values were chosen to be tested, Re=500 and Re=4000. These values were chosen to get both a laminar and a turbulent flow situation. The Drillbench® simulations were done based on the example of a 1500 kg/m^3 drilling fluid presented in chapter 4. With input parameters from this example, the Reynolds number of 500 was found by changing the flow rate to 0.006 m^3/s, while a Reynolds number of 4000 was found at a flow rate of 0.050 m^3/s. The other parameters were kept the same. By reading the values for ECD at rotation rates of 200 RPM, 300 RPM and 600 RPM, and converting these values to the form $\Delta P_{\omega\neq0}/\Delta P_{\omega=0}$ by use of Eq. 5.7, they could be compared to the empirical equations. The result can be seen in **Table 19** for a Reynolds number of 500, and in **Table 20** for a Reynolds number of 4000.

Table 19—Comparison of Drillbench® simulation and $\Delta P_{\omega\neq0}/\Delta P_{\omega=0}$ vs. Re-equations for laminar flow.

Reynolds number = 500 (Laminar flow)			
RPM	**Drillbench® prediction of $\Delta P_{\omega\neq0}/\Delta P_{\omega=0}$**	**Prediction of $\Delta P_{\omega\neq0}/\Delta P_{\omega=0}$ from empirical equations**	**Difference**
200	0.96524	1.62024	67.86 %
300	0.95588	1.51850	58.86 %
600	0.89706	1.96305	118.83 %

Table 20—Comparison of Drillbench® simulation and $\Delta P_{\omega\neq0}/\Delta P_{\omega=0}$ vs. Re-equations for turbulent flow.

Reynolds number = 4000 (Turbulent flow)			
RPM	**Drillbench® prediction of $\Delta P_{\omega\neq0}/\Delta P_{\omega=0}$**	**Prediction of $\Delta P_{\omega\neq0}/\Delta P_{\omega=0}$ from empirical equations**	**Difference**
200	1.07205	1.36430	27.26 %
300	1.10886	1.03573	−6.59 %
600	1.21536	1.95780	61.09 %

From these two tables, it can be seen that the predictions with the empirical equations are closer to the Drillbench® simulation results than was the case for the regressed equation on the form $\Delta P_{\omega\neq0}/\Delta P_{\omega=0}$ vs. RPM, but the prediction is still higher in general.

5.3.2: Comparison With PLR-Equation and a Field Study

This subchapter will compare the results of the regressed equations with the PLR-equation presented in chapter 3, and with the results from the study by Marken et al. (1992), in which the Drillbench® example was based on. In this study, pressure losses in the well at drillstring rotation speeds of 60 RPM and 120 RPM were investigated. As previously described, they used three different mud weights, and made several measurements for all the scenarios. When rotating at 60 RPM, the ratio of the annular pressure losses with rotation to that without rotation ranged between 1.11 and 1.51. At the rotation speed of 120 RPM, the same ratio was between 1.18 and 1.67.

To make use of the PLR-equation, several calculations had to be made. A summary of these calculations can be found in Appendix G. Some of the values had to be assumed because the study provided insufficient information, and these values were the ones related to the eccentricity. It was recommended to use a value of 50%, so this was assumed to be a fair estimate for the calculation. The *n*-variable was calculated by use of the Herschel-Bulkley rheology model, and a log-log plot from a 3 data point oil field approach. **Table 21** contain the calculated values of $\Delta P_{\omega\neq0}/\Delta P_{\omega=0}$ for 60 RPM and 120 RPM, for the three different mud weights.

Table 21—$\Delta P_{\omega\neq0}/\Delta P_{\omega=0}$ vs. RPM–equation compared to PLR-equation and field study.

RPM	Mud weight [kg/m3]	$\Delta P_{\omega\neq0}/\Delta P_{\omega=0}$	PLR	$\Delta P_{\omega\neq0}/\Delta P_{\omega=0}$ range from study
60	1300	0.9931	1.3421	1.11–1.51
60	1500	0.9931	1.3224	1.11–1.52
60	1700	0.9931	1.2971	1.11–1.53
120	1300	1.1931	1.4028	1.18–1.67
120	1500	1.1931	1.3823	1.18–1.68
120	1700	1.1931	1.3384	1.18–1.69

As previously mentioned, there are not enough field data to test the equations on the form $\Delta P_{\omega\neq0}/\Delta P_{\omega=0}$ versus Reynolds number against a field study not used in the regression analysis. The study that was used for comparison with the equation on the form $\Delta P_{\omega\neq0}/\Delta P_{\omega=0}$ vs. RPM did not use rotation speeds above 120 RPM, and is thereby unfitted for verification purposes. However, the PLR-equation can be used. To calculate the required pressure loss ratios, the same input values used in the previous comparison for a 1500 kg/m^3 mud was applied. Two situations were looked at, a laminar flow situation (Re=500), and a turbulent flow situation (Re=4000). The resulting comparison can be seen in **Table 22** and **Table 23.**

Table 22—Comparison of PLR-equation and $\Delta P_{\omega\neq0}/\Delta P_{\omega=0}$ vs. Re-equations for laminar flow.

Reynolds number = 500 (Laminar flow)			
RPM	**Prediction of $\Delta P_{\omega\neq0}/\Delta P_{\omega=0}$ from PLR-equation**	**Prediction of $\Delta P_{\omega\neq0}/\Delta P_{\omega=0}$ by use of empirical equations**	**Difference**
200	1.62694	1.62024	−0.41 %
300	1.66958	1.51850	−9.05 %
600	1.74507	1.96305	12.49 %

Table 23—Comparison of PLR-equation and $\Delta P_{\omega\neq0}/\Delta P_{\omega=0}$ vs. Re-equations for turbulent flow.

Reynolds number = 4000 (Turbulent flow)			
RPM	**Prediction of $\Delta P_{\omega\neq0}/\Delta P_{\omega=0}$ from PLR-equation**	**Prediction of $\Delta P_{\omega\neq0}/\Delta P_{\omega=0}$ by use of empirical equations**	**Difference**
200	1.77534	1.36430	−23.16 %
300	1.82195	1.03573	−43.15 %
600	1.90433	1.95780	2.81 %

From these two tables, it is clear that the empirical equations predict values for $\Delta P_{\omega\neq0}/\Delta P_{\omega=0}$ close to the PLR-equation, with the exception of the 300 RPM-equation for turbulent flow. This is most likely because the data sets used in the regression analysis did not contain data for Reynolds numbers larger than 1300, and would thereby still be within the laminar flow range.

Chapter 6: Discussion and Evaluation of Work

The empirical equations developed in the previous chapters have some limitations. They are made from a small amount of data sets, and do not represent a large enough spread. The data sets are gathered from previous studies on effects of pipe rotation.

6.1 Data Quality

Some errors could have been made in the measurements during the tests, the equipment could have been inaccurately calibrated, or there could have been other factors such as different test conditions for the various runs that would influence the results. A factor that could affect the accuracy of the equations is poorly read data from graphs. There will always be an error when reading values from a graph and the size of each point indicator or the thickness of the line may also influence the read values. The downhole pressure is assumed to be the same as standpipe pressure plus hydraulic pressure, and only the annulus pressures considered. This might also influence the results. The rheology model is a mathematical expression on mud behavior, and does not necessarily depict the actual behavior, although the model that best fits measurements on the mud has been chosen.

6.2 Model Quality

The models were constricted into two types, to fit data representing $\Delta P\omega\neq0/\Delta P\omega=0$ versus RPM, and model to fit data representing $\Delta P_{\omega\neq0}/\Delta P_{\omega=0}$ versus the Reynolds number. Four equations were found, and these equations were tested against simulations in Drillbench®, against a semi-empirical equation from a previous study (Ahmed et al. 2010) on pipe rotation, and for the equation of $\Delta P_{\omega\neq0}/\Delta P_{\omega=0}$ versus RPM, it was tested against data from an independent study.

As can be seen in the figures with the regressed model lines (fig. 17 through fig. 20), there are a great variety in the data points, and consequently the model lines are not accurate for all data points. This is also reflected by the R2-value, which is as low as 0.0355 for the equation describing pressure losses versus Reynolds number for a pipe rotation speed of 600 RPM. The best value of R2 was seen for the equation of pressure losses versus pipe rotation speed of 300 RPM, where the value was 0.9433. These values reflect how well the model line fits the data points used in the regression analysis, and therefore may not be a true reflection on the accuracy of the equation when tested against other field data. This was also seen in the

comparison of the 300 RPM-equation with the PLR-equation, where the largerst deviation appeared.

The difference between model output on the form $\Delta P_{\omega\neq0}/\Delta P_{\omega=0}$ versus RPM was −1.61% at the minimum, with a rotation speed of 60 RPM and a mud weight of 1700 kg/m3, while the largest difference was found to be +121.24% with a rotation rate of 600 RPM and the same mud weight. In general, the difference increased with increasing rotation rate for all mud weights.

The equations on the form $\Delta P_{\omega\neq0}/\Delta P_{\omega=0}$ versus Reynolds number gave a large difference for both a laminar flow (Re=500) and a turbulent flow (Re=4000) with the exception of the equation for a rotation speed of 300 RPM. This predicted a pressure loss ratio with a difference of −6.59% compared to the Drillbench® result for the case of turbulent flow. This is thought to be due to the fact that the data points used in the regression analysis of this rotation speed does not cover Reynolds numbers in the range of turbulent flow.

The $\Delta P_{\omega\neq0}/\Delta P_{\omega=0}$ vs. RPM-equation correlated better with the equation from the study presented in chapter 3, but generally predicted too low pressure losses. The equations on the form $\Delta P_{\omega\neq0}/\Delta P_{\omega=0}$ versus Reynolds number gave satisfying results compared with the predictions from the semi-empirical equation presented in chapter 3, but predicted smaller losses for both laminar and turbulent flow (Re=500 and Re=4000) for rotation speeds of 200 RPM and 300 RPM. The difference increased for both equations when the Reynolds number was 4000. The equation for a rotation rate of 600 RPM gave the best results. This predicted a pressure loss 12.49% above the result found using the equation presented in chapter 3 for the laminar flow, while the difference was only +2.81% for the turbulent flow.

6.3 Future Improvements

All equations developed in present project gave predictions of ECD changes due to pipe rotation closer to field data and already existing equations than the software used in this project. However, the results are not yet satisfying as a simple approach to predict pressure losses. There is a need for more data sets to cover a larger variety of drilling operations and situations, and further testing is still needed. From present project it seems to be hard to get a prediction of pressure losses with the required quality, because there are too many parameters

that will influence the pressure losses, such as eccentricity, borehole diameter, what drill fluid is used, and what flow situation exists.

By gathering larger data sets covering more situations, the equations found in this project can be further developed to reach a final form with predictions close to field measurements. The equations on the form $\Delta P_{\omega \neq 0}/\Delta P_{\omega=0}$ versus Reynolds number require less input values than existing equations, but does not cover enough rotation speeds, so a set of equations covering all situations cannot be made without more time and available data.

The models developed in present project are simple. A more complex model should be considered. This model should be made based on the individual variables, where the final form of the model will be on a multi-variable form when the collected data sets allow this to happen. A model of this type would predict pressure losses more accurately, but still be on a simple form. For this to happen there is a need for larger data sets, and more time.

Chapter 7: Conclusion

On basis of findings and observations made during the present project work, the following conclusions can be drawn:

1. The newest relevant theory has been studied to get an overview of existing knowledge. Areas in need of improvement have been found, and the foundation for a best practice recommendation is set.
2. Four equations was developed based on the data sets gathered in present project. The equations was made through regression analysis of data sets on the simlpe model form $\Delta P_{\omega\neq0}/\Delta P_{\omega=0}$ versus RPM, and $\Delta P_{\omega\neq0}/\Delta P_{\omega=0}$ versus Reynolds number.
3. Equations developed in present project were tested for their accuracy against simulations performed in Drillbench®, against a semi-empirical equation, and against an independent field study.
4. Our model on the form $\Delta P_{\omega\neq0}/\Delta P_{\omega=0}$ versus RPM was found to predict pressure losses well, and close to the result of the semi-empirical equation. Our model predicted higher pressure losses for most rotation speeds compared to the Drillbench® simulation results.
5. The equations on the form $\Delta P_{\omega\neq0}/\Delta P_{\omega=0}$ versus Reynolds were tested for both a laminar flow situation (Re=500) and a turbulent flow situation (Re=4000).
6. To improve the accuracy of the developed equations, further gathering of data sets must be made. There was not a satisfying variation in the data sets. With more data points, the model can be adjusted with greater confidence.
7. The equations developed in present project did not cover all drilling situations. Equations on the form $\Delta P_{\omega\neq0}/\Delta P_{\omega=0}$ versus Reynolds number was only developed for rotation speeds of 200 RPM, 300 RPM, and 600 RPM. To develop equations for more rotation speeds, more time and field data is necessary.
8. To improve the model, a more complex model should be made. This can be done by looking at the variables individually, and collect these variables into a multi-variable model when the data allows for it to happen.

References

Ahmed, R. and Miska, S. 2008. Experimental Study and Modeling of Yield Power-Law Fluid Flow in Annuli with Pipe Rotation. Paper IADC/SPE 112604 presented at the IADC/SPE Drilling Conference, Orlando, Florida, USA, 4–6 March.

Ahmed, R., Enfis, M., and Miftah-El-Kheir, H. et al. 2010. The Effect of Drillstring Rotation on Equivalent Circulation Density: Modeling and Analysis of Field Measurements. Paper SPE 135587 presented at the SPE Annual Technical Conference and Exhibition, Florence, Italy, 19–22 September.

Ward, C. and Andreassen, A. 1997. Pressure-While-Drilling Data Improve Reservoir Drilling Performance. Paper SPE 37588 presented at the SPE/IADC Drilling Conference, Amsterdam, 4–6 March.

Bode, D.J., Noffke, R.B., and Nickens, H.V. 1989. Well-Control Methods and Practices in Small-Diameter Wellbores. Paper SPE 19526 presented at the SPE Annual Technical Conference and Exhibition, San Antonio, Texas, USA, 8–11 October.

Charlez, A., Easton, M., and Morrice, G. et al. 1998. Validation of Advanced Hydraulic Modeling using PWD Data. Paper OTC 8804 presented at the Offshore Technology Conference, Houston, 4–7 May.

Delwiche, R.A., Lejeune, M.W.D and Mawet, P.F.B.N, et al. 1992. Slimhole Drilling Hydraulics. Paper SPE 24596 presented at the Annual Technical Conference and Exhibition of the Society of Petroleum Engineers, Washington, DC, 4–7 October.

Diaz, H., Miska, S., and Takach, N. et al. 2004. Modeling of ECD in Casing Drilling Operations and Comparison with Experimental and Field Data. Paper IADC/SPE 87149 presented at the IADC/SPE Drilling Conference, Dallas, 2–4 March.

Haige, W., Yinao, S., and Yangmin, B. et al. 2000. Experimental Study of Slimhole Annular Pressure Loss and Its Field Applications. Paper IADC/SPE 59265 presented at the IADC/SPE Drilling Conference, New Orleans, 23–25 February.

Hansen, S.A. and Sterri, N. 1995. Drill Pipe Rotation Effects on Frictional Pressure Losses in Slim Annuli. Paper SPE 30488 presented at the SPE Annual Technical Conference and Exhibition, Dallas, 22–25 October.

Hansen, S.A., Rommetveit, R., and Sterri, N. et al. 1999. A New Hydraulics Model for Slim Hole Drilling Applications. Paper SPE/IADC 57579 presented at the SPE/IADC Middlie East Drilling Technology Conference, Abu Dhabi, 8–10 November.

Hemphill, T., Bern, P., and Rojas, J.C. et al. 2007. Field Validation of Drillpipe Rotation Effects on Equivalent Circulation Density. Paper SPE 110470 presented at the SPE Annual Technical Conference and Exhibition, Anaheim, California, USA, 11–14 November.

Isambourg, P., Brangetto, M., and Bertin, D.L. 1998. Field Hydraulic Tests Improve HPHT Drilling Safety and Performance. Paper SPE 59527 presented at the SPE Annual Technical Conference and Exhibition, New Orleans, 27–30 September.

Marken, C.D., He, X. and Saasen, A. 1992. The Influence of Drilling Conditions on Annular Pressure Losses. Paper SPE 24598 presented at the Annual Technical Conference and Exhibition of the of the Society of Petroleum Engineers, Washington, DC, 4–7 October.

McCann, R.C., Quigley, M.S., Slater K.S. et al. 1993. Effects of High-Speed Pipe Rotation on Pressure in Narrow Annuli. Paper SPE 26343 presented at the SPE Annual Technical Conference and Exhibition, Houston, 3–6 October.

New Mexico Tech University. 2012. Swab/Surge pressures, http://infohost.nmt.edu/~petro/faculty/Kelly/Swab.pdf (accessed 07 March 2012).

OilGasGlossary. 2012. Oil and Gas Glossary, http://oilgasglossary.com/friction-loss.html (accessed 13 March).

Skalle, P. 2010. Drilling Fluid Engineering. © 2010 Pål Skalle & Ventus Publishing ApS, ISBN 978-87-7681-552-3. http://bookboon.com/no/laereboker/geoscience-eboker/.

Skjold, T. L. 2011. Report on impact of borehole dynamics on well stability in depleted reservoirs. Technical report, Norwegian University of Science and Technology, Trondheim, Norway (unpublished).

SPT Group. 2012. Advanced drilling engineering and operation, www.sptgroup.com/upload/documents/Brochures/drillbench5.pdf (downloaded 12 February 2012).

International Research Institute of Stavanger (IRIS). 2012. Features of the Ullrigg Drilling and Well Centre, http://iris.no/internet/ullrigg.nsf/wvDocID/B0F12B566AB3B01DC125770C0030D5D5 (accessed 05 April 2012).

Abbreviations

BETA	Baker Hughes Experimental Test Area
BHP	Bottomhole Pressure
CMC	Carboxyl Methyl Cellulose
DBS	DB Stratabit Ltd
ECD	Equivalent Circulation Density
ERD	Extended Reach Driling
ESD	Equivalent Static Density
HPHT	High Pressure High Temperature
LPM	Liters per minute
MD	Measured depth
PPG	Punds per gallon
PVT	Pressure, Volume, Temperature
PWD	Pressure-While-Drilling
RPM	Revolutions per minute
SG	Standard gravity
TD	Total depth
TVD	True Vertical Depth
UKCS	United Kingdom Continental Shelf
YP	Yield point

Nomenclature

N.1 Roman

a	Acceleration, L/t^2, m/s^2
a_{pipe}	Pipe acceleration, L/t^2, m/s^2
$A_{ann,effective}$	Effective annulus area, L^2, m^2
$A_{pipe,effective}$	Effective pipe area, L^2, m^2
$c_{cuttings,average}$	Average cuttings concentration of volume fraction of particles, dimensionless
D_h	Borehole diameter, L, m
D_p	Pipe diameter, L, m
D_{TJ}	Tool joint diameter, L, m
E_i	Effective eccentricity over a wellbore section, dimensionless
g	Gravity constant, L/t^2, m/s^2
k	Diameter ratio between drillpipe and borehole wall, dimensionless
L	Length, L, m
L_i	Length of a wellbore section, L, m
m	Mass, m, kg
n	Herschel-Bulkley fluid behaviour index, dimensionless
OD_{pipe}	Outer diameter of pipe, L, m
PLR	Pressure loss ratio, dimensionless
Q	Flow rate, L^3/t, m^3/s
R	Rod radius, L, m
R^2	Coefficient of determination, dimensionless
Re_{eff}	Effective Reynolds number, dimensionless
Ta	Taylor number, dimensionless
U	Mean annular velocity (in chapter 3), L/t, m/s
U	Axial averaged velocity, L/t, m/s
z	Depth, L, m

N.2 Greek

$(dP/dL)_\omega$	Pressure loss with pipe rotation, m/Lt^2, Pa

$(dP/dL)_{\omega=0}$	Pressure loss with no pipe rotation, m/Lt^2, Pa
$\Delta p_{acceleration}$	Pressure losses resulting from acceleration, m/Lt^2, Pa
$\Delta p_{cuttings}$	Pressure losses caused by cuttings, m/Lt^2, Pa
$\Delta p_{friction,annular}$	Annular pressure losses caused by friction, m/Lt^2, Pa
$\Delta p_{rotation}$	Pressure losses resulting from pipe rotation, m/Lt^2, Pa
$\Delta p_{surge\&swab}$	Pressure losses caused by surge and swab effects, m/Lt^2, Pa
ΔP	Pressure losses, m/Lt^2, Pa
$\Delta P_{\omega=0}$	Pressure losses without rotation, m/Lt^2, Pa
$\Delta P_{\omega\neq0}$	Pressure losses with rotation, m/Lt^2, Pa
$\Delta P_{\omega\neq0}/\Delta P_{\omega=0}$	Pressure losses with rotation over pressure losses without rotation, dimensionless
ε_{ave}	Average eccentricity, dimensionless
μ_{app}	Apparent viscosity, m/Lt, Pa·s
ρ	Density, m/L^3, kg/m^3
$\rho_{cuttings}$	Cuttings density, m/L^3, kg/m^3
$\rho_{cuttings,average}$	Average cuttings density, m/L^3, kg/m^3
ρ_{mud}	Density of mud, m/L^3, kg/m^3
$\tau_{w,lam}$	Average wall shear stress, m/Lt^2, Pa
τ_y	Herschel-Bulkley yield stress, m/Lt^2, Pa
ω	Angular rod rotation speed, 1/t, rad/s
$\omega R/U$	Ratio between rod tangential velocity and mud axial averaged velocity, dimensionless

Appendix A: Well Data from SPE 24596

This appendix contain copies of graphs and tables from the study by Delwiche et al. (1992) which were used for data sets acquisition in this project. **Fig. 21** contains important parameters for the 578P1172 well, and **Fig. 22** is a graph representing the effect of rod rotation speed on annular pressure losses for this well. In **Fig. 23,** a graph of the pressure losses versus flow rate and rotation speed can be seen. **Fig. 24** contain important parameters for well 425P1210, and **Fig. 25** is a graph of the rod rotation speed effects on annular pressure losses for this well, while **Fig. 26** show the pressure loss plotted against flow rate and rotation speed. As for **Fig. 27,** it hold the most important well parameters for 425P2078, with **Fig. 28** as the graphical presentation of this wells rod rotation speed effects on annular pressure losses, and **Fig. 29** the pressure loss versus flow rate and rotation speed.

Total : 578P1172

BHA

Casing	6,625	168,3 Øe (mm)
		148,02i (mm)
Shoe depth	937 m	
Open hole	5,875	149,2 Øe (mm)
Total depth	1180m	
Drill pipe	CHD134	127,02e (mm)
		114,32i (mm)
		104,82i upset(mm)

MUD

FANN 600	34	SG	1,27
FANN 300	20	T°	38
FANN 200	15		
FANN 100	9		
FANN 6	2	gel 0	1
FANN 3	2	gel 10	3
	pétrole	si	
AV	17	0,017	
osw			
n	0,765	0,765	
K	0,170	0,081	
bin			
YP	6	2,874	
PV	14	0,014	

Fig. 21—Well 578P1172 characteristics.

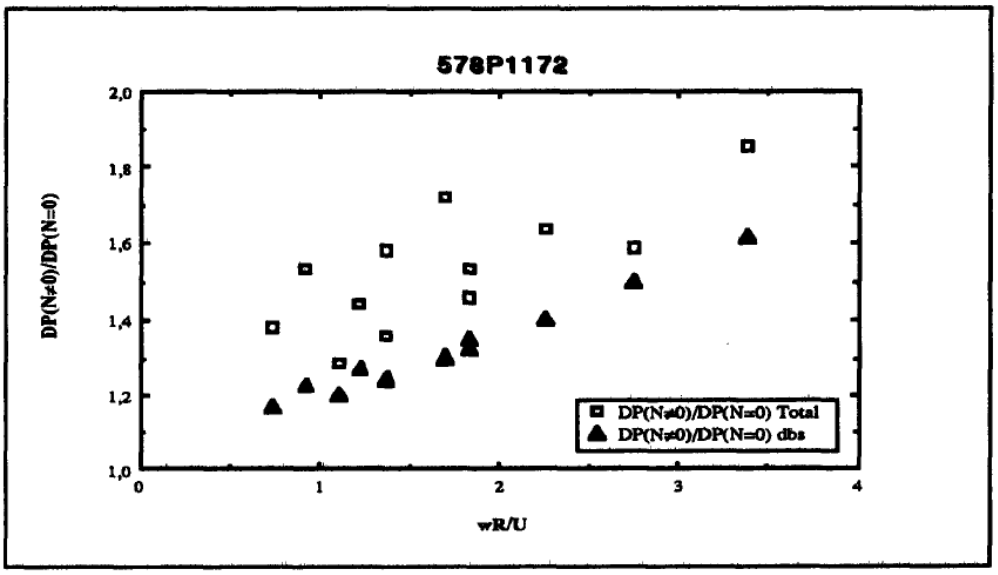

Fig. 22—Effect of rod rotation speeds on annular pressure losses for well 578P1172.

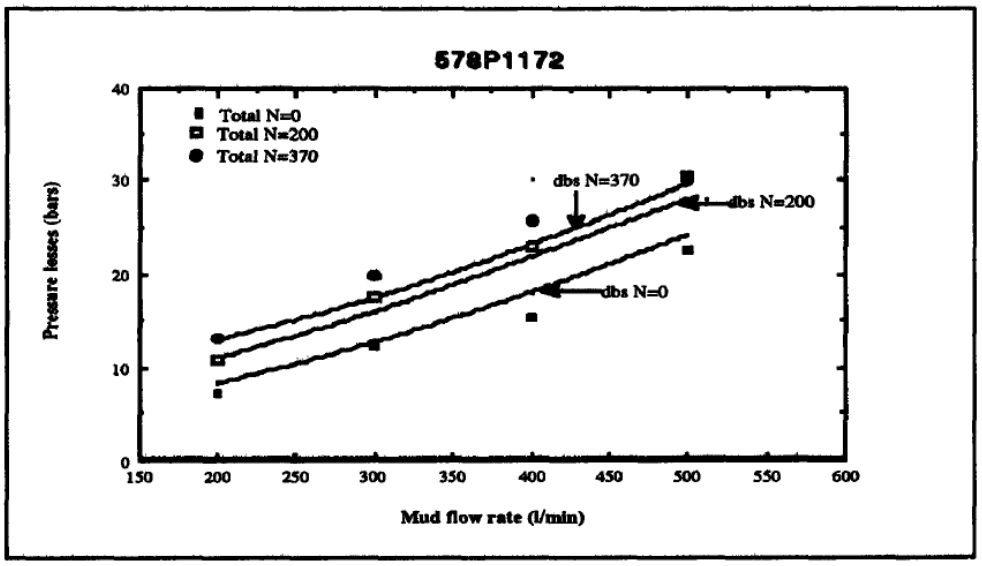

Fig. 23—Total pressure losses in function of mud flow rates and rotation speed for well 578P1172

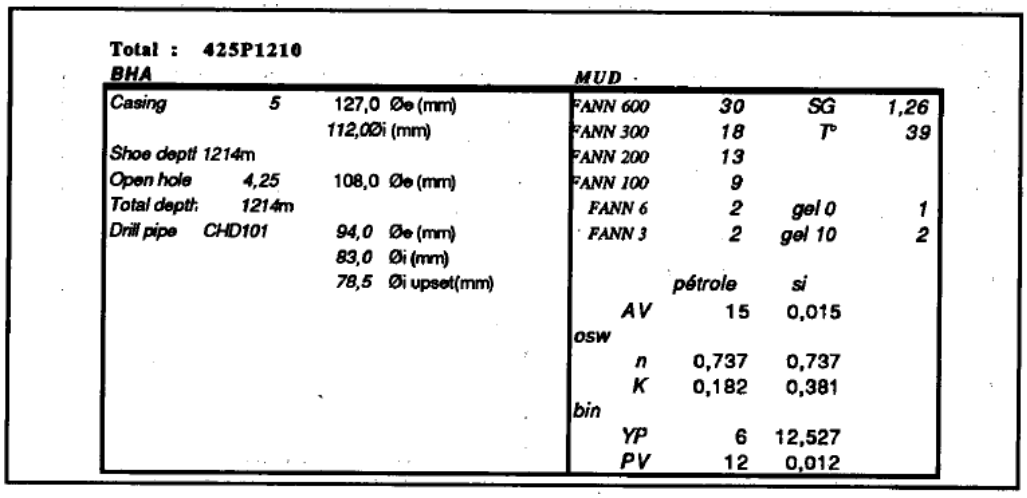

Total : 425P1210

BHA

Casing	5	127,0	Øe (mm)
		112,02	Øi (mm)
Shoe depth	1214m		
Open hole	4,25	108,0	Øe (mm)
Total depth:	1214m		
Drill pipe	CHD101	94,0	Øe (mm)
		83,0	Øi (mm)
		78,5	Øi upset(mm)

MUD

FANN 600	30	SG	1,26
FANN 300	18	T°	39
FANN 200	13		
FANN 100	9		
FANN 6	2	gel 0	1
FANN 3	2	gel 10	2
	pétrole	si	
AV	15	0,015	
osw			
n	0,737	0,737	
K	0,182	0,381	
bin			
YP	6	12,527	
PV	12	0,012	

Fig. 24—Well 425P1210 characteristics.

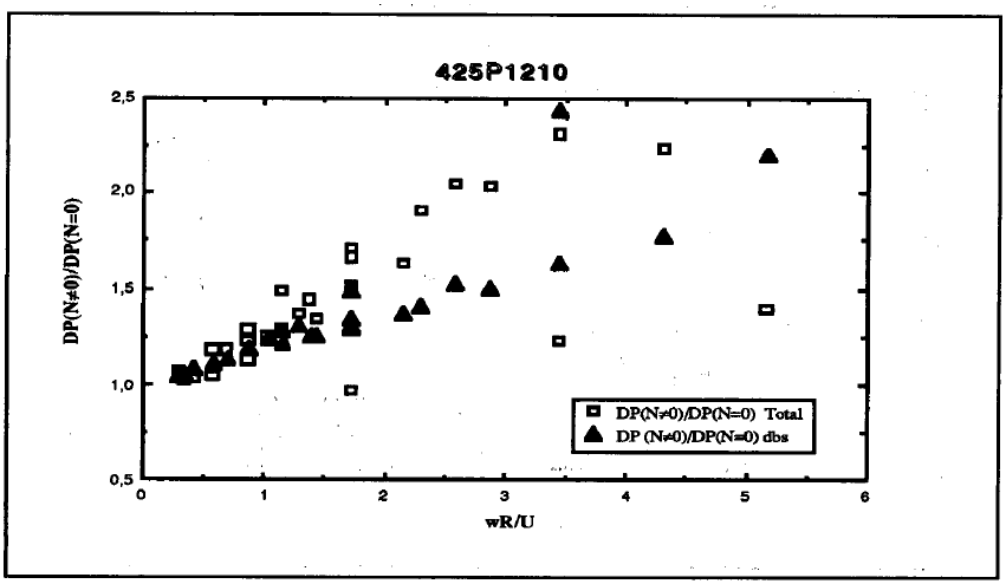

Fig. 25—Effect of rod rotation speeds on annular pressure losses for well 425P1210.

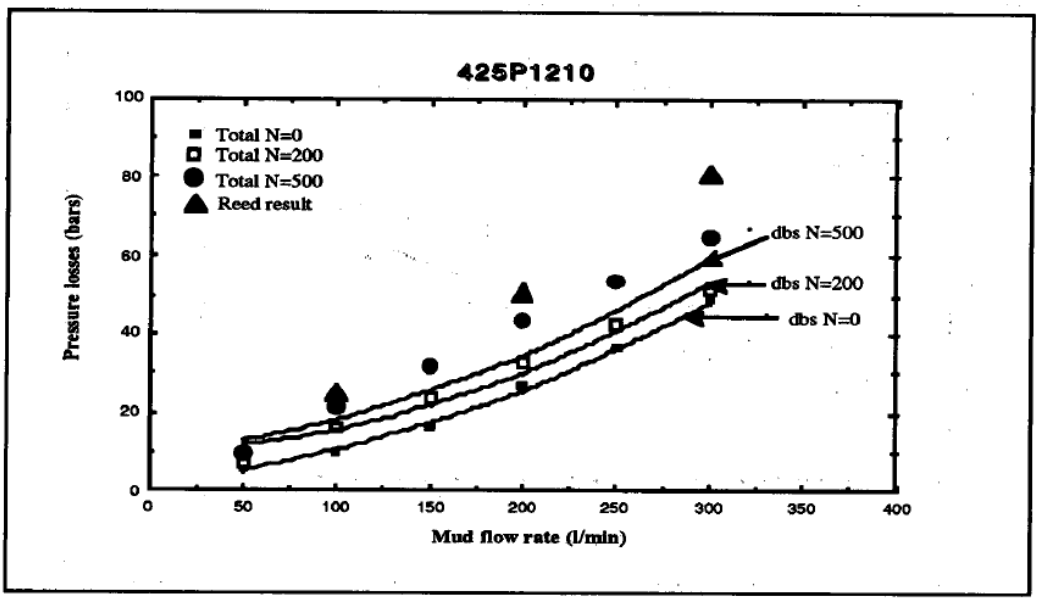

Fig. 26—Total pressure losses in function of mud flow rates and rotation speed for well 425P1210

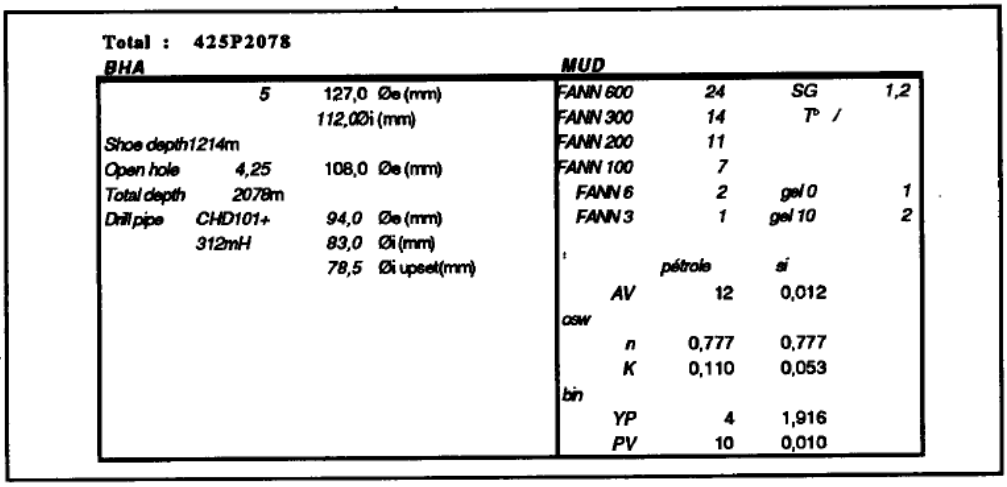

Total : 425P2078

BHA				MUD			
	5	127,0	Øe (mm)	FANN 600	24	SG	1,2
		112,00i	(mm)	FANN 300	14	T° /	
Shoe depth1214m				FANN 200	11		
Open hole	4,25	108,0	Øe (mm)	FANN 100	7		
Total depth	2078m			FANN 6	2	gel 0	1
Drill pipe	CHD101+	94,0	Øe (mm)	FANN 3	1	gel 10	2
	312mH	83,0	Øi (mm)				
		78,5	Øi upset(mm)		pétrole	si	
				AV	12	0,012	
				csw			
				n	0,777	0,777	
				K	0,110	0,053	
				bin			
				YP	4	1,916	
				PV	10	0,010	

Fig. 27—Well 425P2078 characteristics.

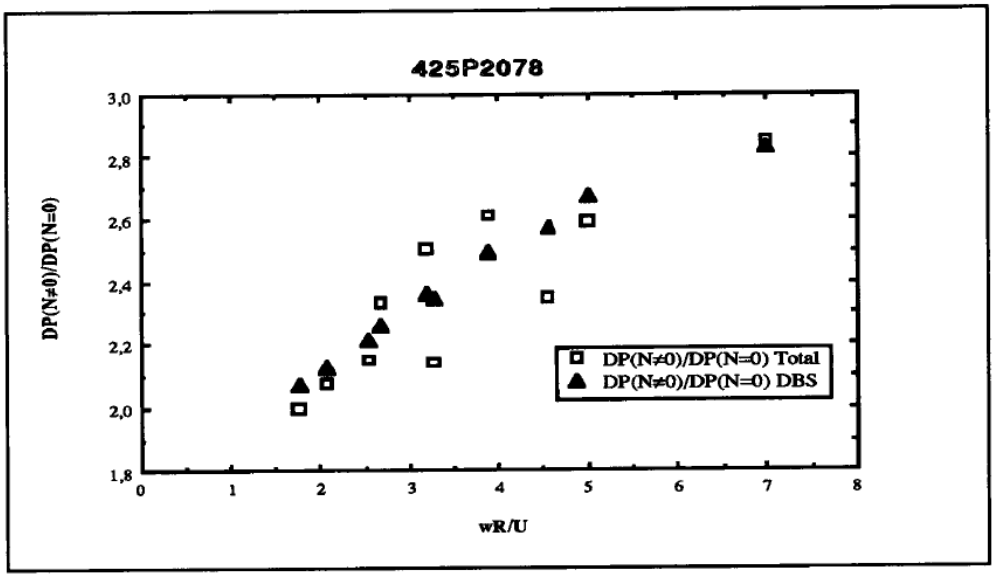

Fig. 28—Effect of rod rotation speeds on annular pressure losses for well 425P2078.

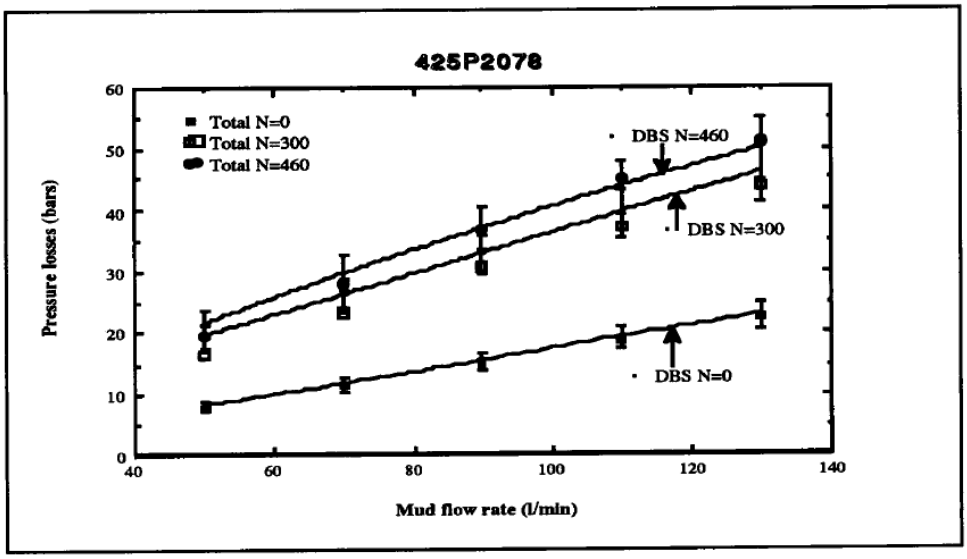

Fig. 29—Total pressure losses in function of mud flow rates and rotation speed for well 425P2078

Appendix B: Well Data from SPE 59265

This appendix contain copies of the graphs and tables from the study of Haige et al. (2000) which were used for data sets acquisition in this project. **Fig. 30** shows the graph of drillpipe rotational effects on annular pressure losses for three fluid velocities that was presented in this study of well Miao 1-40.

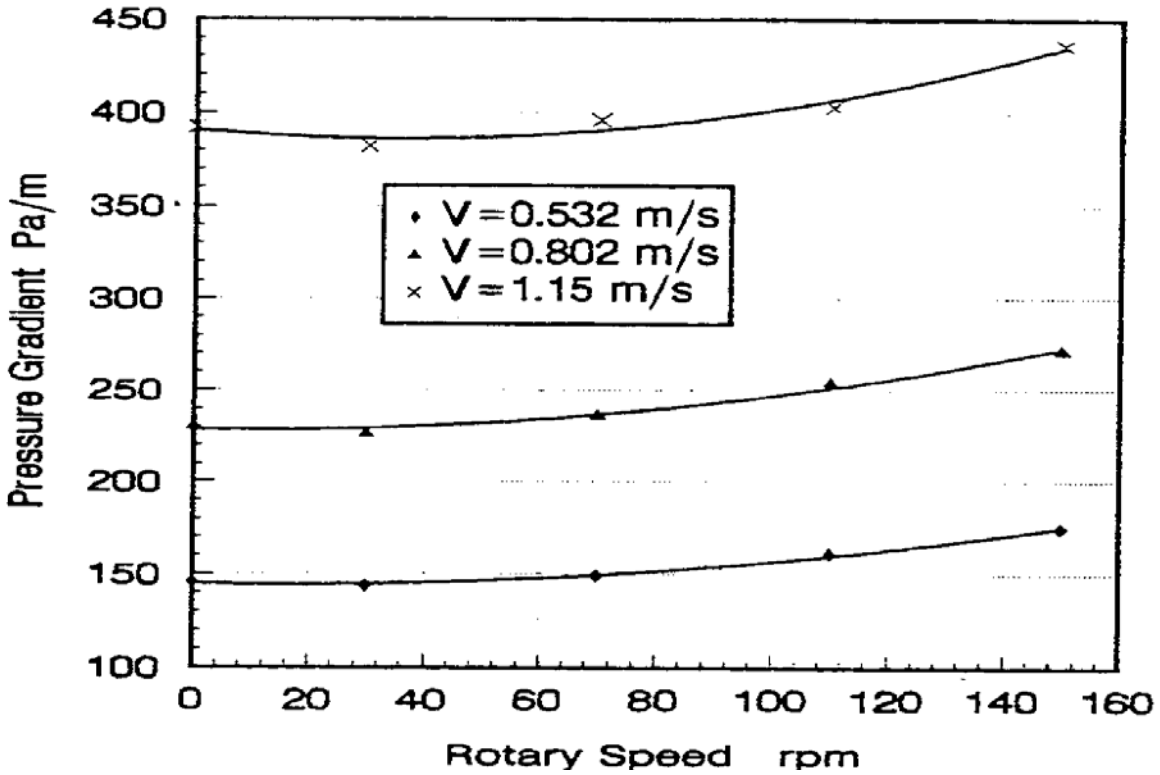

Fig. 30—Effects of drillpipe rotation speed on annular pressure losses in the Miao 1-40 well.

Appendix C: Well Data from SPE 87149

This appendix contain copies of the graphs and tables from the study by Diaz et al. (2004) which were used for data sets acquisition in this project. **Fig. 31** contains properties used in calculation with water as the drilling fluid, while **Fig. 32** contains the same information for the two other drilling fluids, Mud A and Mud B.

Table 2. Fluid and Cuttings Properties			
Fluid		Cutting	
Density	Viscosity	Specific Gravity	Diameter
ppg	cp		in
8.33	1	2.6	0.25

Fig. 31—Fluid and cuttings properties with water as drilling fluid

Table 3. Average Properties of Muds							
Fluid	Density	Fann Viscometer Reading					
	ppg	600	300	200	100	6	3
A	8.7	11	7	6	4	1	1
B	9.8	35	23	18	12	3	3

Fig. 32—Fluid properties for Mud A and Mud B drilling fluids

The measured and calculated data was in this study presented for three different flow rates, and for each of these flow rates measurements were done with the three various drilling fluids, water, Mud A and Mud B. In **Fig. 33,** a graph showing BHP versus rotary speed with water as drilling fluid is presented. The hole diameter was 12.715 in., the outer casing diameter was 11.75 in., the true depth was 86.26 m, and the flow rate was 0.022 m^3/s. **Fig. 34** show the same graph, but with a new flow rate of 0.028 m^3/s. In **Fig. 35,** the graph is shown for a flow rate of 0.035 m^3/s. In **Fig. 36,** the graph is showing BHP versus rotary speed with Mud A as drilling fluid. Again, the hole diameter was 12.715 in., the outer casing diameter was 11.75 in., and the true depth was 86.26 m. In this figure, the flow rate was 0.022 m^3/s. **Fig. 37** show the same graph with a flow rate of 0.028 m^3/s, and **Fig. 38** show the graph for the situation of a 0.035 m^3/s flow rate. **Fig. 39** contains a graph of the BHP versus rotary speed with a flow rate of 0.022 m^3/s, and with Mud B as the drilling fluid. Here as well the hole diameter is 12.715 in., the casing OD is 11.75 in., and the depth is at 86.26 m. **Fig. 40 and Fig. 41** show the same graph, but with a flow rate of 0.028 m^3/s and 0.035 m^3/s respectively.

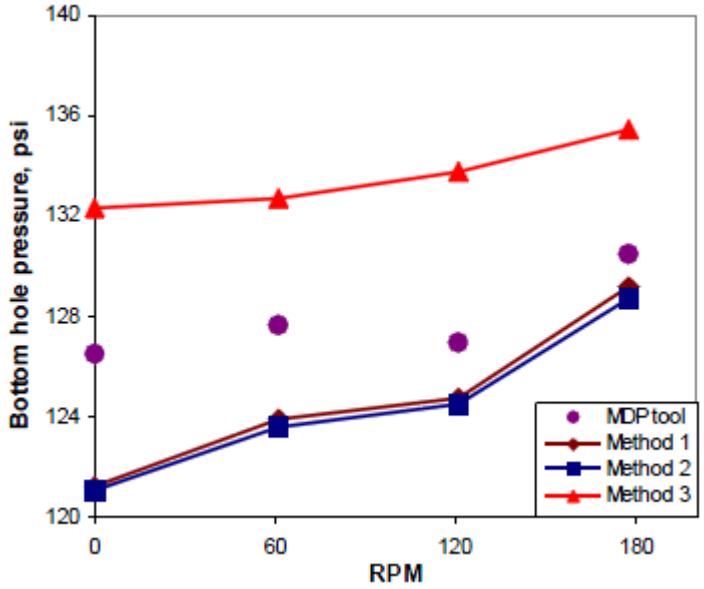

Fig. 33—Bottomhole pressure versus rotary speed. Drilling fluid is water. D_h=12.715 in., OD=11.75 in., TD=85.26 m, Q=0.022 m^3/s.

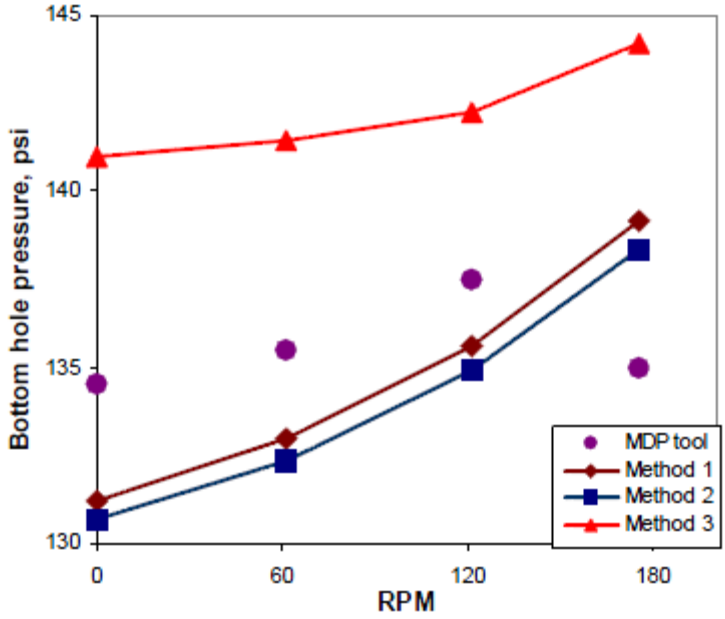

Fig. 34—Bottomhole pressure versus rotary speed. Drilling fluid is water. D_h=12.715 in., OD=11.75 in., TD=86.26 m, Q=0.028 m^3/s.

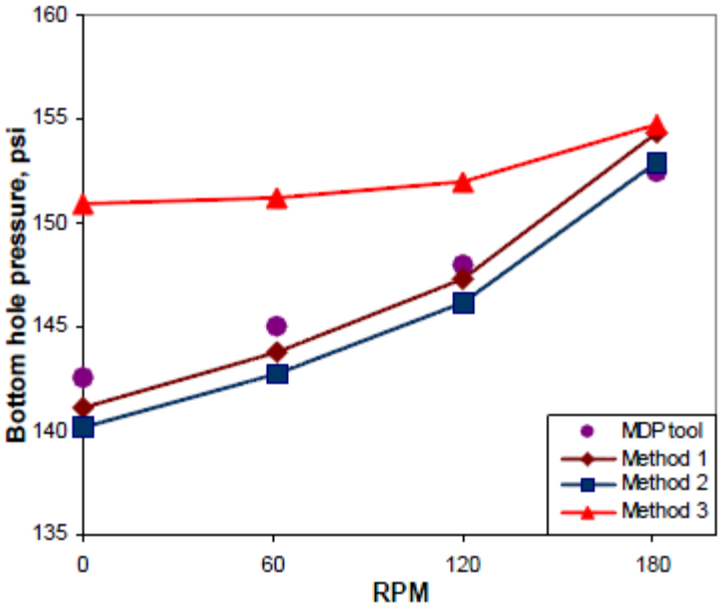

Fig. 35—Bottomhole pressure versus rotary speed. Drilling fluid is water. D_h=12.715 in., OD=11.75 in., TD=86.26 m, Q=0.035 m^3/s.

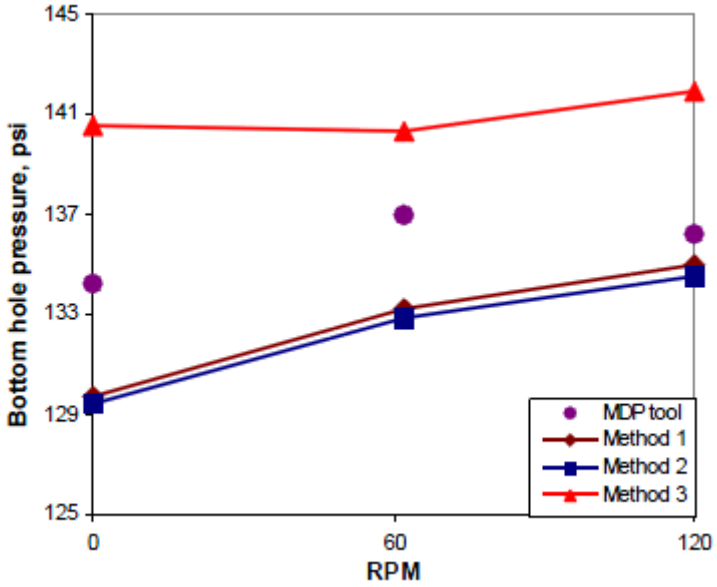

Fig. 36—Bottomhole pressure versus rotary speed. Drilling fluid is Mud A. D_h=12.715 in., OD=11.75 in., TD=86.26 m, Q=0.022 m^3/s.

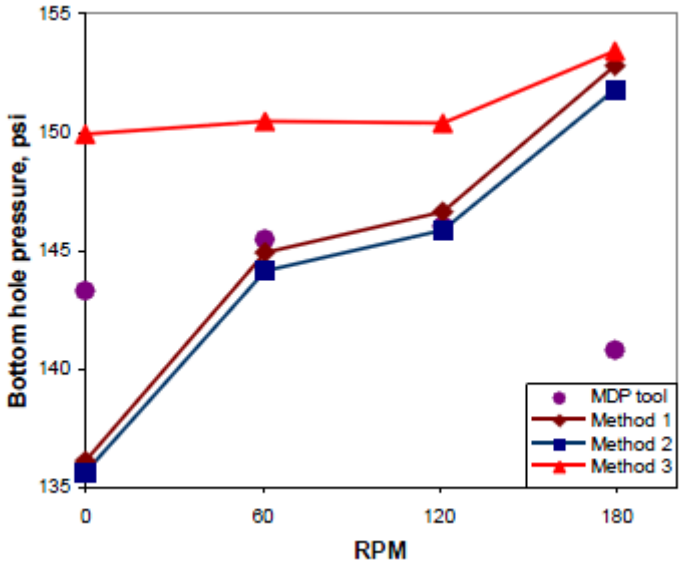

Fig. 37—Bottomhole pressure versus rotary speed. Drilling fluid is Mud A. D_h=12.715 in., OD=11.75 in., TD=86.26 m, Q=0.028 m^3/s.

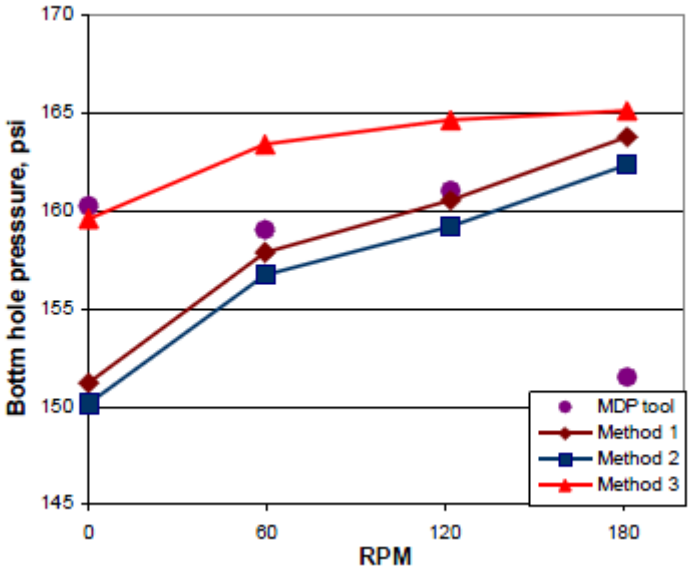

Fig. 38—Bottomhole pressure versus rotary speed. Drilling fluid is Mud A. D_h=12.715 in., OD=11.75 in., TD=86.26 m, Q=0.035 m^3/s.

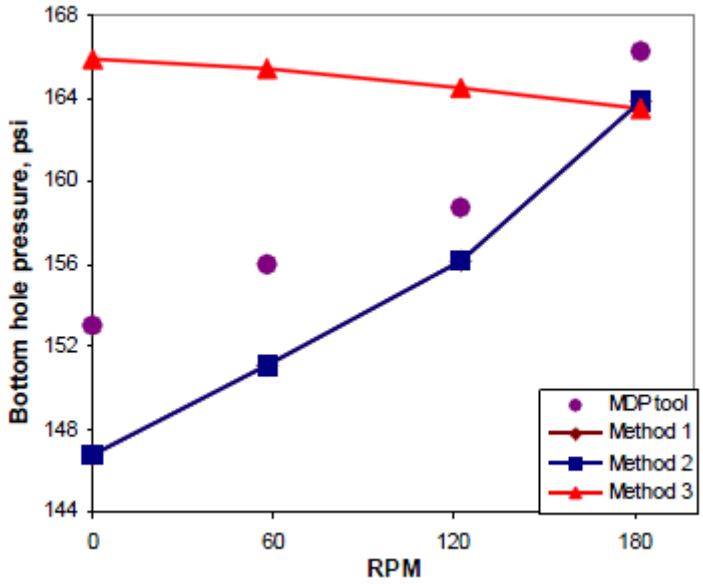

Fig. 39—Bottomhole pressure versus rotary speed. Drilling fluid is Mud B. D_h=12.715 in., OD=11.75 in., TD=86.26 m, Q=0.022 m^3/s.

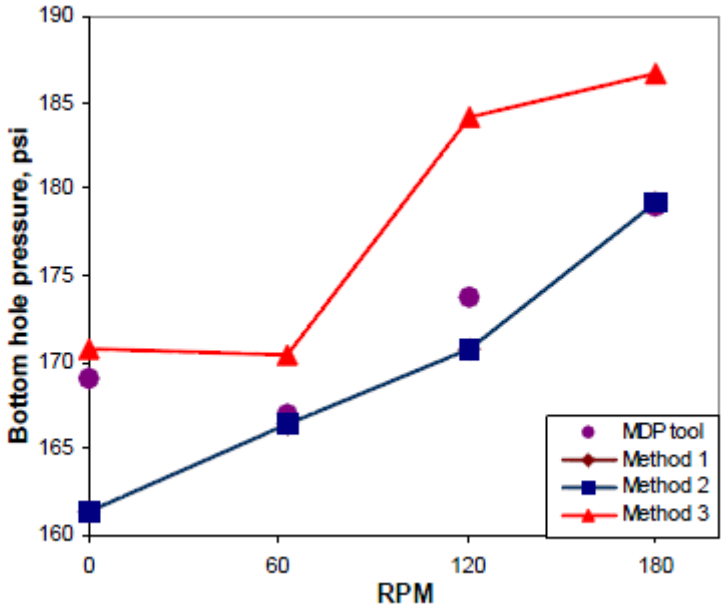

Fig. 40—Bottomhole pressure versus rotary speed. Drilling fluid is Mud B. D_h=12.715 in., OD=11.75 in., TD=86.26 m, Q=0.028 m^3/s.

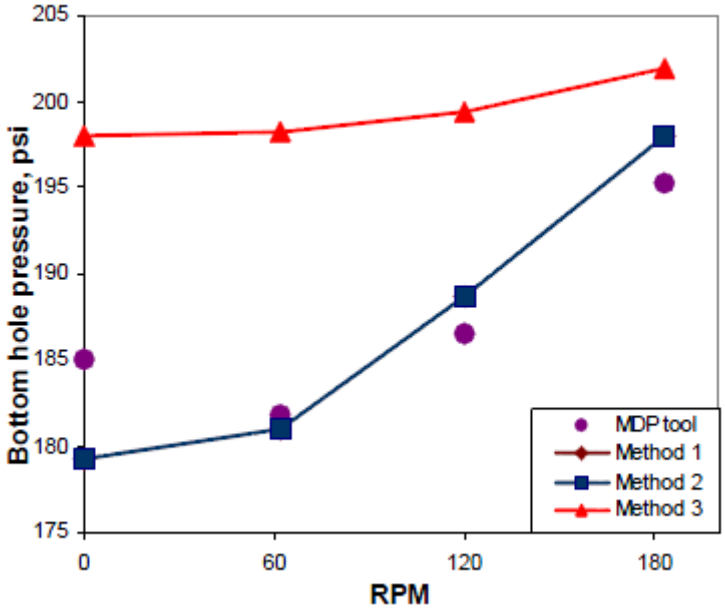

Fig. 41—Bottomhole pressure versus rotary speed. Drilling fluid is Mud B. D_h=12.715 in., OD=11.75 in., TD=86.26 m, Q=0.035 m^3/s.

Appendix D: Well Data from SPE 19526

This appendix contain a copy of the drilling data from Bode et al. (1989), used in the development of empirical equations. **Fig. 42** contain a graph presented in this study, showing the Reynolds number plotted against the annular pressure losses with rotation over that of no rotation, for three different rotation speeds.

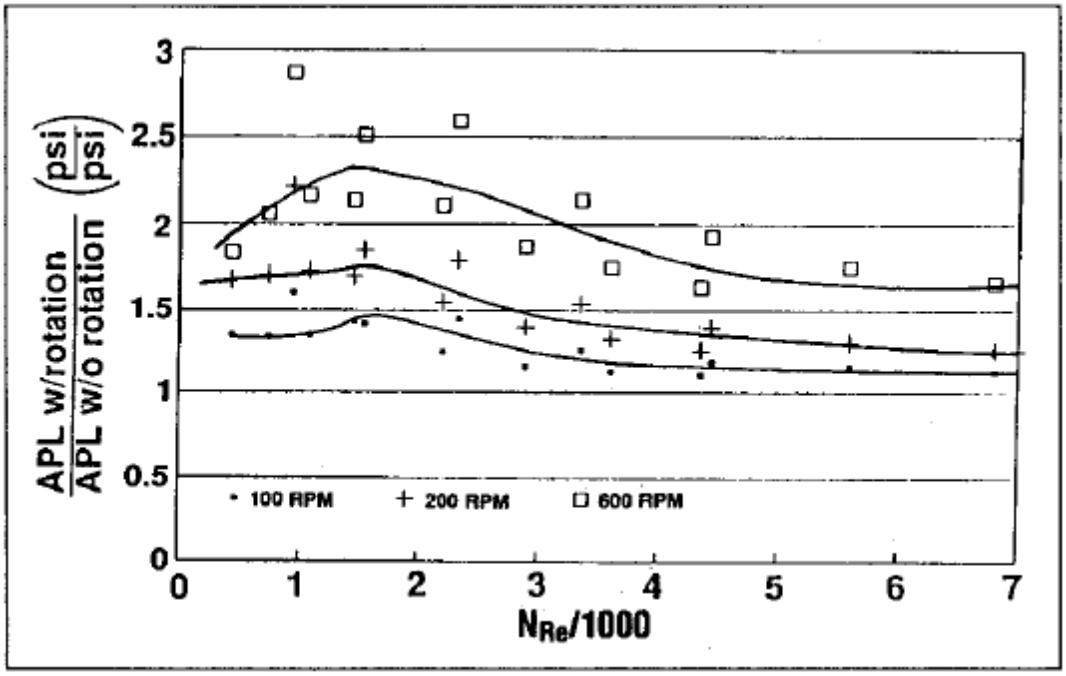

Fig. 42—Annular pressure losses with rotation over annular pressure losses without rotation plotted against the Reynolds number for three rotation speeds.

Appendix E: Well Data from SPE 110470

This appendix contains a copy of 22/30c-G4 well data from Hemphill et al. (2007). The data is presented in **Fig. 43,** and show the data on the form *Measured Change in ECD vs. Drillpipe Rotation Speed*. Two data sets were gathered from this figure, called Elf 8.75-in A and Elf 8.75-in B.

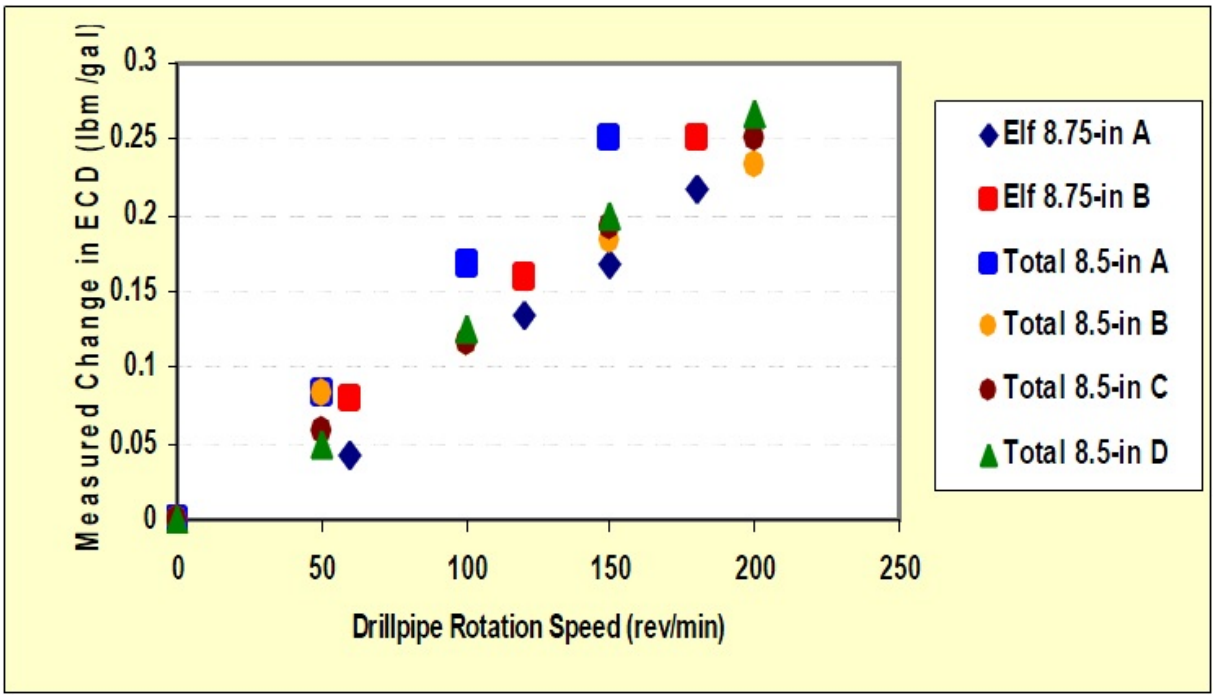

Fig. 43—Measured Change in ECD plotted against RPM for ELF 8.75-in A and ELF 8.75-in B

Appendix F: Well Data from SPE 26343

This appendix contains a copy of the graph representing the data sets from the SHDT.1 well in McCann et al. (1993). The graph is presented in **Fig. 44,** and show the annular pressure vs. flow rate for rotation rates of 300 and 600 RPM.

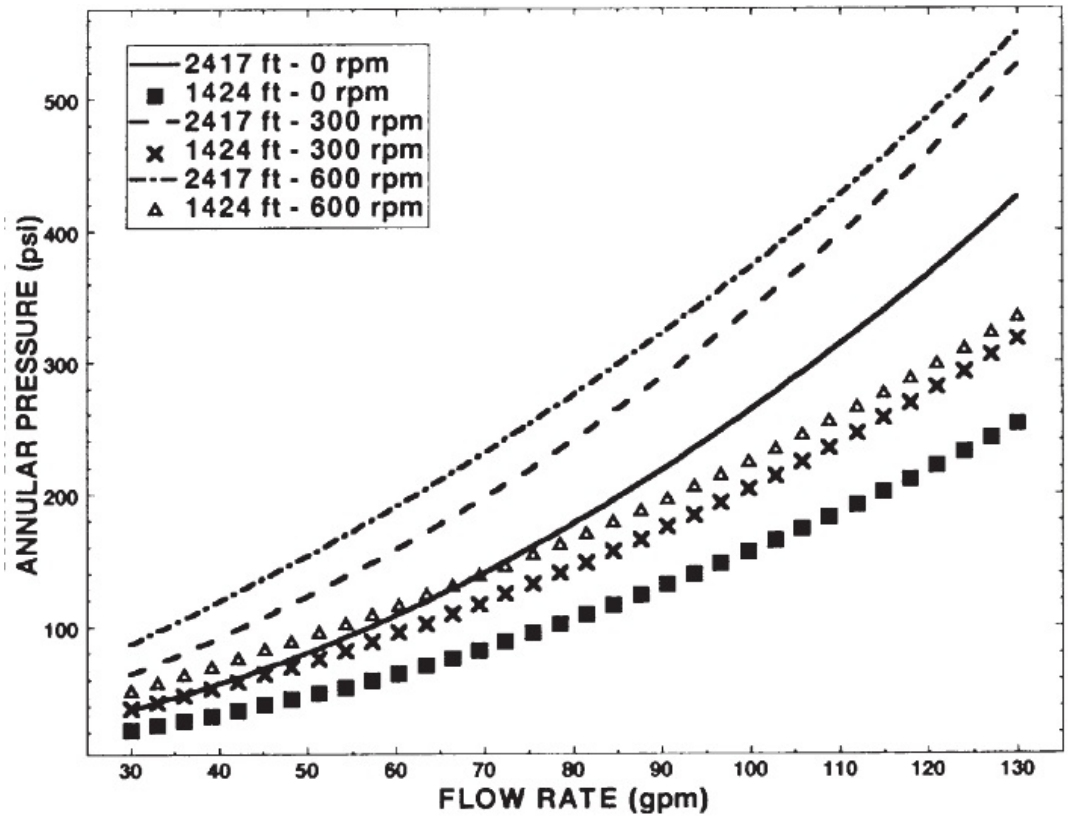

Fig. 44—Annular pressure plotted against flow rate. RPM is 300 and 600

Appendix G: Input Values for Calculations with PLR-Equation

This appendix contains a summary of the input values used when doing calculations with the PLR-equation. **Table 24** contain input values for the 1300 kg/m^3 mud, **Table 25** contain input values for the 1500 kg/m^3 mud, and **Table 26** contain input values for the 1700 kg/m^3 mud. In **Fig. 45,** the resulting log-log plot from the Herschel-Bulkley 3 point oil field approach for calculation of *n* is shown for the 1300 kg/m^3 mud, and in **Fig. 46 and Fig. 47,** the same plot is shown for the 1500 kg/m^3 and 1700 kg/m^3 mud respectively.

Table 24—Input values in PLR-calculations. Mud weight is 1300 kg/m^3, rotations speed 120 RPM to the left, 60 RPM to the right

Parameter	Value	Units
ρ	1300	kg/m^3
τ_y	8.6184	Pa
U	1.9735	m/s
ε_{ave}	0.5	
n	0.3449	
Ta	175 000	
Re_{eff}	755	
k	0.7647	
D_p	0.1651	m
D_h	0.2159	m
ω	120	RPM
μ_{app}	0.0470	Pa·s
MD	2000	m
L_i	xxxx	m
E_i	xxxx	
D_{TJ}	0.1651	m
$\tau_{w,lam}$	53.6259	Pa

Parameter	Value	Units
ρ	1300	kg/m^3
τ_y	8.6184	Pa
U	1.9735	m/s
ε_{ave}	0.5	
n	0.3449	
Ta	43 700	
Re_{eff}	755	
k	0.7647	
D_p	0.1651	m
D_h	0.2159	m
ω	60	RPM
μ_{app}	0.0470	Pa·s
MD	2000	m
L_i	xxxx	m
E_i	xxxx	
D_{TJ}	0.1651	m
$\tau_{w,lam}$	53.6259	Pa

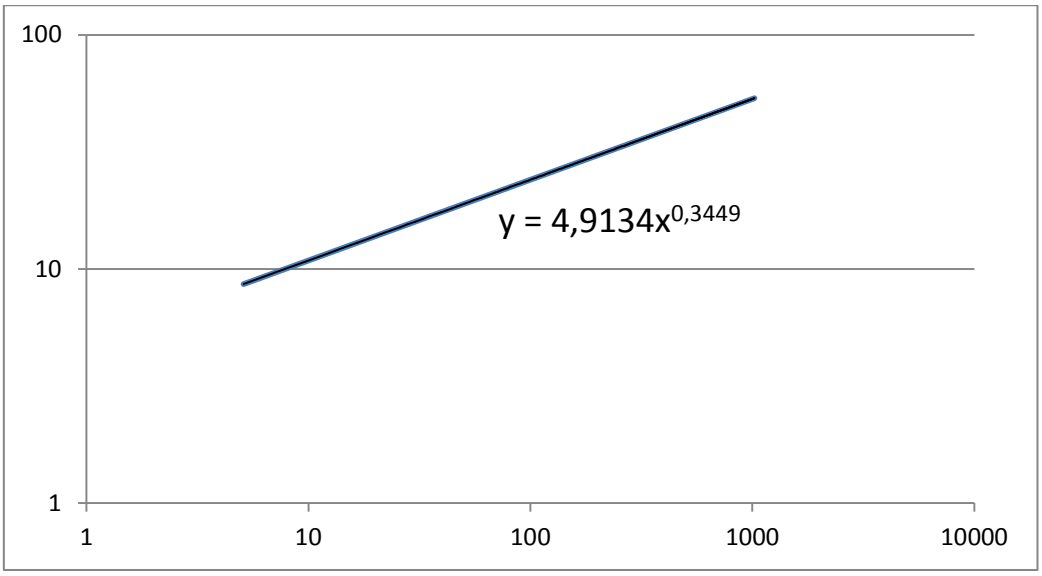

Fig. 45—Log-log plot from Herschel-Bulkley 3 point oil field approach calculation of n by use of 1300 kg/m^3 mud

Table 25—Input values in PLR-calculations. Mud weight is 1500 kg/m^3, rotation speed 120 RPM to the left, 60 RPM to the right

Parameter	Value	Units
ρ	1500	kg/m^3
τ_y	11.4913	Pa
U	1.9735	m/s
ε_{ave}	0.5	
n	0.3432	
Ta	133 000	
Re_{eff}	660	
k	0.7647	
D_p	0.1651	m
D_h	0.2159	m
ω	120	RPM
μ_{app}	0.0620	Pa·s
MD	2000	m
L_i	xxxx	m
E_i	xxxx	
D_{TJ}	0.1651	m
$\tau_{w,lam}$	70.8628	Pa

Parameter	Value	Units
ρ	1500	kg/m^3
τ_y	11.4913	Pa
U	1.9735	m/s
ε_{ave}	0.5	
n	0.3432	
Ta	33 200	
Re_{eff}	660	
k	0.7647	
D_p	0.1651	m
D_h	0.2159	m
ω	60	RPM
μ_{app}	0.0620	Pa·s
MD	2000	m
L_i	xxxx	m
E_i	xxxx	
D_{TJ}	0.1651	m
$\tau_{w,lam}$	70.8628	Pa

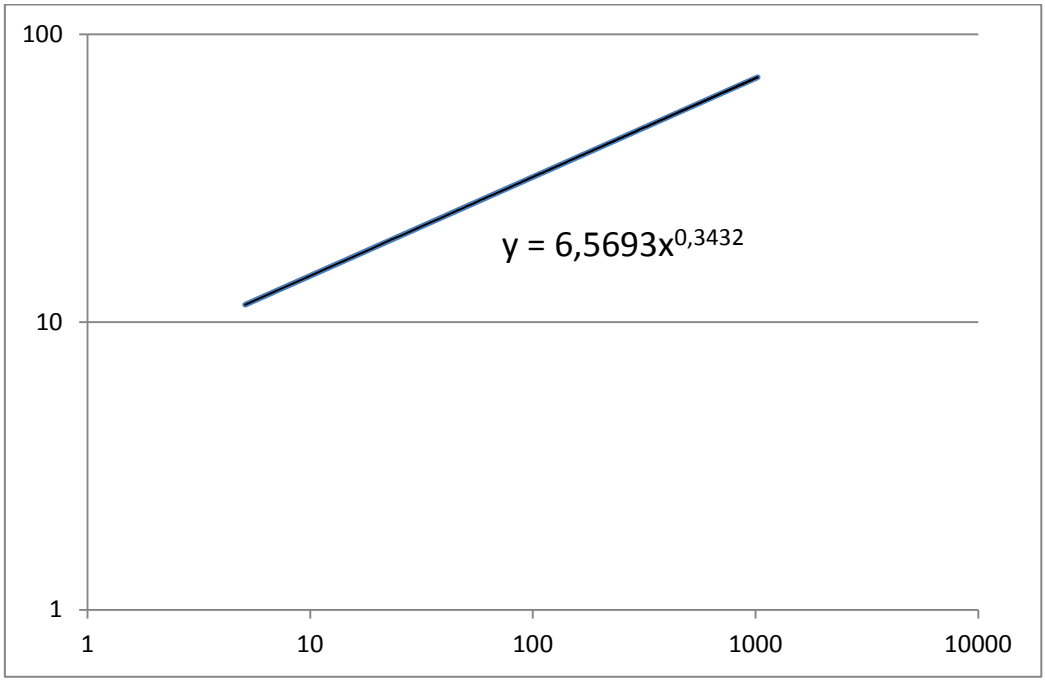

Fig. 46—Log-log plot from Herschel-Bulkley 3 point oil field approach calculation of n by use of 1500 kg/m^3 mud

Table 26—Input values in PLR-calculations. Mud weight is 1700 kg/m^3, rotation speed 120 RPM to the left, 60 RPM to the right

Parameter	Value	Units
ρ	1700	kg/m^3
τ_y	15.3217	Pa
U	1.9735	m/s
ε_{ave}	0.5	
n	0.3458	
Ta	60 200	
Re_{eff}	553	
k	0.7647	
D_p	0.1651	m
D_h	0.2159	m
ω	120	RPM
μ_{app}	0.0840	Pa·s
MD	2000	m
L_i	xxxx	m
E_i	xxxx	
D_{TJ}	0.1651	m
$\tau_{w,lam}$	95.7605	Pa

Parameter	Value	Units
ρ	1700	kg/m^3
τ_y	15.3217	Pa
U	1.9735	m/s
ε_{ave}	0.5	
n	0.3458	
Ta	22 500	
Re_{eff}	553	
k	0.7647	
D_p	0.1651	m
D_h	0.2159	m
ω	60	RPM
μ_{app}	0.0840	Pa·s
MD	2000	m
L_i	xxxx	m
E_i	xxxx	
D_{TJ}	0.1651	m
$\tau_{w,lam}$	95.7605	Pa

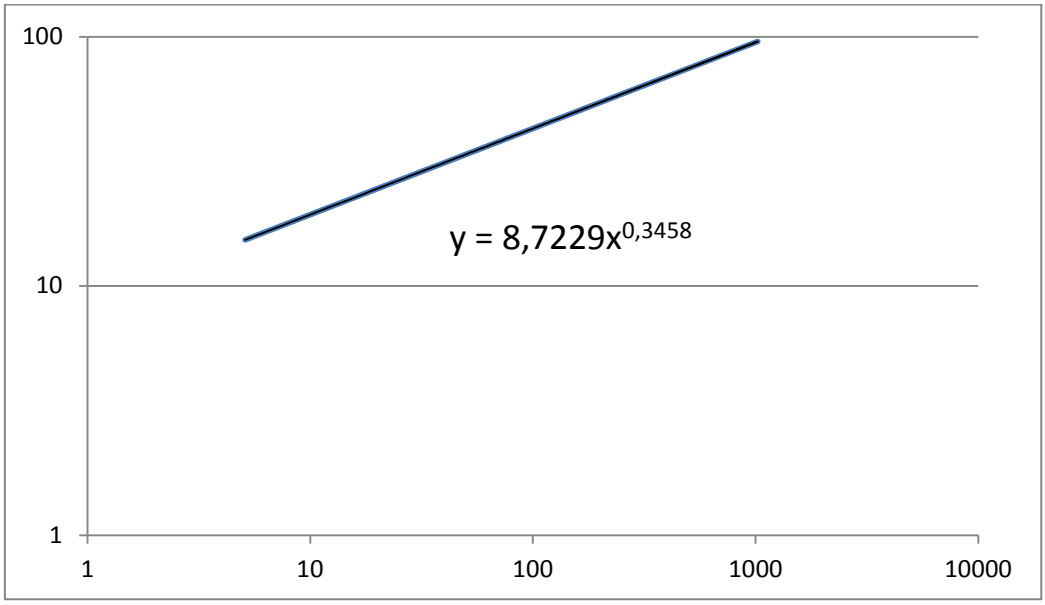

Fig. 47—Log-log plot from Herschel-Bulkley 3 point oil field approach calculation of n by use of 1700 kg/m^3 mud

Appendix H: Calculation Inputs

This appendix contains the input values used in calculations throughout the project. **Table 27** contains input values used for calculations needed in transforming data from **Fig. 23** of Appendix A into the required form.

Table 27—Input values for 578P1172 calculations

ρ [kg/m^3]	1270	1270	1270	1270
v [m/s]	0.19096	0.28644	0.38192	0.47741
d_h [m]	0.02223	0.02223	0.02223	0.02223
D_o [m]	0.14923	0.14923	0.14923	0.14923
D_i [m]	0.127	0.127	0.127	0.127
n	0.765	0.765	0.765	0.765
K	0.081	0.081	0.081	0.081
A [m^2]	0.01746	0.01746	0.01746	0.01746
Q [m^3/s]	0.00333	0.00500	0.00667	0.00833
μ_{eff} [Pa·s]	0.02936	0.02669	0.02495	0.02367
Re	184	303	432	569

Table 28 contains the input values used for calculations needed in transforming data from **Fig. 26** of Appendix A into the required form.

Table 28—Input values for 425P1210 calculations

ρ [kg/m^3]	1260	1260	1260	1260	1260	1260
v [m/s]	0.07606	0.15212	0.22818	0.30424	0.38030	0.45636
d_h [m]	0.01395	0.01395	0.01395	0.01395	0.01395	0.01395
D_o [m]	0.10795	0.10795	0.10795	0.10795	0.10795	0.10795
D_i [m]	0.094	0.094	0.094	0.094	0.094	0.094
n	0.737	0.737	0.737	0.737	0.737	0.737
K	0.381	0.381	0.381	0.381	0.381	0.381
A [m^2]	0.01096	0.01096	0.01096	0.01096	0.01096	0.01096
Q [m^3/s]	0.00083	0.00167	0.00250	0.00333	0.00417	0.005
μ_{eff} [Pa·s]	0.13783	0.11486	0.10325	0.09572	0.09027	0.08604
Re	10	23	39	56	74	93

Table 29 contains the input values used for calculations needed in transforming data from **Fig. 29** of Appendix A into the required form.

Table 29—Input values for 425P2078 calculations

ρ [kg/m^3]	1200	1200	1200	1200	1200
v [m/s]	0.07606	0.10648	0.13691	0.16733	0.19776
d_h [m]	0.01395	0.01395	0.01395	0.01395	0.01395
D_o [m]	0.10795	0.10795	0.10795	0.10795	0.10795
D_i [m]	0.094	0.094	0.094	0.094	0.094
n	0.777	0.777	0.777	0.777	0.777
K	0.053	0.053	0.053	0.053	0.053
A [m^2]	0.01096	0.01096	0.01096	0.01096	0.01096
Q [m^3/s]	0.00083	0.00117	0.00150	0.00183	0.00217
μ_{eff} [Pa·s]	0.02240	0.02078	0.01965	0.01879	0.01810
Re	57	86	117	149	183

In **Table 30,** the input values for calculations performed on the data read from **Fig. 44** of Appendix F is seen.

Table 30—Input values for SHDT.1 calculations

ρ [kg/m^3]	1000	1000	1000	1000	1000	1000	1000	1000	1000	1000	1000
v [m/s]	0.652	0.869	1.086	1.303	1.52	1.737	1.955	2.172	2.389	2.606	2.823
d_h [m]	0.018	0.018	0.018	0.018	0.018	0.018	0.018	0.018	0.018	0.018	0.018
D_o [m]	0.112	0.112	0.112	0.112	0.112	0.112	0.112	0.112	0.112	0.112	0.112
D_i [m]	0.094	0.094	0.094	0.094	0.094	0.094	0.094	0.094	0.094	0.094	0.094
τ_{300} [Pa]	20	20	20	20	20	20	20	20	20	20	20
γ_{300} [s^{-1}]	511	511	511	511	511	511	511	511	511	511	511
A [m^2]	0.0029	0.0029	0.0029	0.0029	0.0029	0.0029	0.0029	0.0029	0.0029	0.0029	0.0029
Q [m^3/s]	0.0019	0.0025	0.0032	0.0038	0.0044	0.005	0.0057	0.0063	0.0069	0.0076	0.0082
μ_{eff} [Pa·s]	0.0391	0.0391	0.0391	0.0391	0.0391	0.0391	0.0391	0.0391	0.0391	0.0391	0.0391
Re	298	398	497	597	696	796	895	995	1094	1194	1293

Unit Conversion Factors

Below is a table with conversion factors from oil field units to SI metric units **(Table 31),** and a table with conversion factors from other units to SI metric units **(Table 32).**

Table 31—Conversion factors from oil field units to SI units

Oil Field Units	Conversion Factor	SI Metric Unit
ft	3.048000 E−01	m
in	2.540000 E−02	m
lbm/gal (PPG)	1.198264 E+02	kg/m^3
ft^2	9.290304 E−02	m^2
lb/ft	1.488189 E+00	kg/m
cP	1.000000 E−03	Pa·s
psi	6.894760 E+03	Pa
ft/min	5.080000 E−03	m/s
gal/min (GPM)	6.309020 E−05	m^3/s
psi/ft	2.262060 E+04	Pa/m

Table 32—Conversion factors from other units SI units

Other Units	Conversion Factor	SI Metric Unit
LPM	6.000000 E−04	m^3/s
cm	1.000000 E−02	m
SG	1.000000 E+03	kg/m^3
°C	°C + 273.15	°K
bar	1.000000 E+04	Pa
mm	1.000000 E−03	m